

Development and preclinical evaluation of new theranostic anti-CXCR4 radiopharmaceuticals

THESIS

submitted by

Karen LEYS

Laboratory for Radiopharmaceutical Research

Academic promotor: Prof. Dr. Guy BORMANS

Co-promotor: Dr. Frederik CLEEREN

LEUVEN

Academic year 2019-2020

Copyright

© Copyright by KU Leuven

Without written permission of the promotor(s) and the author it is forbidden to reproduce or adapt in any form or by any means any part of this publication.

A written permission of the promotor is also required to use the methods, products, schematics and programs described in this work for industrial or commercial use, and for submitting this publication in scientific contests.

“De auteur en de promotor(en) geven omwille van confidentialiteit geen rechtstreekse toelating deze scriptie voor consultatie beschikbaar te stellen en delen ervan te kopiëren voor persoonlijk gebruik. Enkel bij voorafgaande toestemming van KU Leuven zal deze scriptie gebruikt mogen worden. Elk ander gebruik valt onder de beperkingen van het auteursrecht, in het bijzonder met betrekking tot de verplichting uitdrukkelijk de bron te vermelden bij het aanhalen van de resultaten uit deze scriptie. De auteur en de promotor(en) behouden zich het recht delen van deze scriptie aan te wenden voor wetenschappelijke publicaties.”

Acknowledgements

First and foremost, I would like to thank my promotor, Dr. prof. Guy Bormans, for welcoming me at the Radiopharmaceutical lab and for giving me a chance to learn. The knowledge that I have gathered this past year has been indispensable. I have always wanted to do research and this experience has cemented that belief, above all thanks to his counselling and eagerness to help.

Next, I would like to thank my supervisor, Dr. Frederik Cleeren, for his continuous help and guidance during this thesis. This work would not have been the same without his invaluable input. I am grateful for all of his help; it was a significant factor in enabling me to hone my skills. He trusted me to handle the challenges that were given to me, yet was always very understanding and helpful whenever I had any questions.

I would also like to thank the lab of Radiopharmacy as a whole, for making me feel so welcome; from the moment I started working there in September, until the very end of my internship. They all welcomed my questions about everything and anything graciously and were always ready to lend me a helping hand whenever I needed it. I would like to thank a few people in particular, whom have had to bear the brunt of my questions yet were always ready to help: Ivan, Pieter and Irwin.

Lastly, I would like to thank my parents, family and friends for standing by me, not only during the past year, but always. Their support has been invaluable in my life and I would not be the same person without them.

TABLE OF CONTENT

Copyright.....	
Acknowledgements.....	
List of abbreviations.....	I
Samenvatting.....	III
Summary.....	IV
1. INTRODUCTION.....	1
1.1. NUCLEAR MEDICINE.....	1
1.2. RADIONUCLIDES IN NUCLEAR MEDICINE.....	2
1.2.1. Single photon emission computed tomography (SPECT)	4
1.2.2. Positron emission tomography (PET)	4
1.2.3. Advantages of PET over SPECT.....	5
1.2.4. Fluorine-18 and gallium-68; the most used PET radionuclides in clinical practice.....	5
1.2.4.1. Fluorine-18.....	5
1.2.4.2. Gallium-68.....	5
1.2.4.3. Fluorine-18 vs gallium-68.....	6
1.2.5. Therapeutic radionuclides.....	6
1.2.5.1. Lutetium-177.....	8
1.2.5.2. Actinium-225.....	8
1.3. THERANOSTICS.....	8
1.4. CHEMOKINE RECEPTOR CXCR4.....	9
1.4.1. Chemokines and chemokine receptors.....	9
1.4.2. CXC chemokine receptor type 4	10
1.5. CURRENT RADIOPHARMACEUTICALS FOR THE CXCR4 RECEPTOR.....	11
1.5.1. Radiotracers	11
1.5.2. [⁶⁸Ga]Ga-Pentixafor	12
1.5.3. [¹⁷⁷Lu]Lu-Pentixather.....	13
1.6. DV1-K-(DV3) PEPTIDE AS CXCR4 ANTAGONIST.....	14
2. AIMS/OBJECTIVES.....	16
3. MATERIALS AND METHODS	18
3.1. MATERIALS	18
3.2. SYNTHESIS AND PURIFICATION OF RESCA-DV1-K-(DV3).....	19
3.3. FITC-DV1-K-(DV3) SYNTHESIS.....	20
3.4. LABELLING WITH STABLE ISOTOPES.....	21
3.4.1. ^{nat}F⁻-AIF-labelling of NODA-MP-NCS	21
3.4.2. ^{nat}Ga³⁺-labelling of NOTA-DV1-K-(DV3)	22
3.4.3. ^{nat}Ga³⁺-labelling of DOTA-DV1-K-(DV3)	22

3.4.4.	^{nat} Lu ³⁺ -labelling of DOTA-DV1-K-(DV3)	22
3.4.5.	^{nat} La ³⁺ -labelling of DOTA-DV1-K-(DV3)	23
3.5.	LYOPHILIZATION	23
3.6.	AFFINITY TESTS	23
3.7.	CALCIUM-BINDING ASSAY	24
3.8.	QUALITY CONTROL SYSTEM	26
3.9.	RADIOSYNTHESIS OF [¹⁸ F]AIF-NOTA-DV1-K-(DV3)	27
3.10.	PHARMACOKINETICS OF [¹⁸ F]AIF-NOTA-DV1-K-(DV3)	28
3.10.1.	μPET/CT	28
3.10.2.	Biodistribution study	29
4.	RESULTS	30
4.1.	SYNTHESIS AND PURIFICATION OF RESCA-DV1-K-(DV3)	30
4.2.	FITC-DV1-K-(DV3) SYNTHESIS	31
4.3.	LABELLING WITH STABLE ISOTOPES	33
4.3.1.	^{nat} F ⁻ -AIF-labelling of NODA-MP-NCS	33
4.3.2.	^{nat} Ga ³⁺ -labelling of NOTA-DV1-K-(DV3)	33
4.3.3.	^{nat} Ga ³⁺ -labelling of DOTA-DV1-K-(DV3)	35
4.3.4.	^{nat} Lu ³⁺ -labelling of DOTA-DV1-K-(DV3)	36
4.3.5.	^{nat} La ³⁺ -labelling of DOTA-DV1-K-(DV3)	37
4.4.	AFFINITY TESTS	38
4.5.	CALCIUM-BINDING ASSAY	39
4.6.	QUALITY CONTROL SYSTEM	40
4.7.	PHARMACOKINETICS OF [¹⁸ F]AIF-NOTA-DV1-K-(DV3)	43
4.7.1.	μPET/CT	43
4.7.2.	Biodistribution study	44
5.	DISCUSSION	46
5.1.	DV1-K-(DV3) PEPTIDE	46
5.2.	FUNDAMENTAL RESEARCH AND PRECLINICAL EVALUATION	48
5.3.	FUTURE STEPS	50
6.	CONCLUSION	52
7.	LITERATURE CITED	53

List of abbreviations

AA(s)	amino acid(s)
ACN	acetonitrile
AE(s)	adverse event(s)
BSA	bovine serum albumin
CD184	cluster of differentiation 184
CXCL12	C-X-C Motif Chemokine Ligand 12
CXCR4	CXC chemokine Receptor type 4
DCM	dichloromethane
DIPEA	N-Ethyldiisopropylamine
DMF	dimethylformamide
DOTA	1,4,7,10-tetraazacyclododecane-1,4,7,10-tetraacetic acid
DMSO	dimethyl sulfoxide
e ⁻	electron
e ⁺	positron
EC	electron capture
ECL	extracellular loop
ESI	electrospray ionization
FITC	fluorescein isothiocyanate
FOV	field of view
HATU	2-(7-Aza-1H-benzotriazole-1-yl)-1,1,3,3-tetramethyluronium hexafluorophosphate
HBSS	Hank's Balanced Salt Solution
HEPES	4-(2-hydroxyethyl)-1-piperazineethanesulfonic acid
HIV	human immunodeficiency virus
HPV-8	human herpesvirus-8
HRMS	high-resolution mass spectrometry
IC ₅₀	half-maximal inhibitory concentration
IT	isomeric transition
ICL	intracellular loop
LC-HRMS	liquid chromatography high-resolution mass spectrometry
mSv	millisievert
μPET	microPET
MoSAIC	Molecular Small Animal Imaging Center
Mr	molecular mass
MRI	magnetic resonance imaging

n	neutron
NODA	1,4,7-triazacyclononane-1,4-diacetic acid
NODA-MP-NCS	NODA 7-meta phenyl-isothiocyanate
NOTA	1,4,7-triazacyclononane-1,4,7-triacetic acid
p	proton
PD	pharmacodynamics
PET	positron emission tomography
p.i.	post injection
PK	pharmacokinetics
POM	proof of mechanism
PRRT	peptide receptor radionuclide therapy
PTFE	polytetrafluorethylene
PVDF	polyvinylidene fluoride
QC	quality control
RA	rheumatoid arthritis
RESCA	restrained complexing agent
Rt	retention time
SAR(s)	serious adverse event(s)
SD	standard deviation
SDF-1	stromal-derived-factor-1
SPECT	single-photon emission computed tomography
SUV	standardized uptake value
$t_{1/2}$	half life
TFA	trifluoroacetic acid
Tis	tri-isopropyl silane
TOF	time-of-flight
Tris base	tris(hydroxymethyl)aminomethane
TRNT	targeted radionuclide therapy
UPLC	ultra-performance liquid chromatography
ν_e	electron neutrino
$\bar{\nu}_e$	antineutrino
vMIP-II	viral Macrophage Inflammatory Protein-II

Samenvatting

Achtergrond: Onderzoek heeft aangetoond dat de CXCR4 receptor een belangrijke rol speelt bij verschillende kankertypes. Bestaande beeldvorming en therapie zijn niet afdoende voor de nood die er vandaag is. Een theranostische aanpak die specifiek is voor deze receptor zou een waardevolle bijdrage leveren aan de opsporing en behandeling van verschillende kankertypes. DV1-K-(DV3), een peptide bestaande uit D-aminozuren en CXCR4-antagonist, is een interessant vector molecule voor de ontwikkeling van radiofarmaceutische preparaten in een “theranostische setting” en zal voor het eerst getest worden als vectormolecule.

Doel: In deze thesis werd het peptide DV1-K-(DV3) geëvalueerd als vector molecule voor de ontwikkeling van zowel diagnostische en therapeutische radiofarmaceutische preparaten. Er werden verschillende testen mee gedaan om na te gaan of DV1-K-(DV3) geschikt is als theranostische vector met CXCR4 als doelwit.

Methoden: Verschillende modificaties werden toegepast op het peptide, zoals synthese van een FITC-derivaat, een aluminiumfluoride-RESCA-derivaat, aluminiumfluoride en gallium NOTA derivaten en lutetium en lanthanum DOTA derivaten. Daarna werden de constructen gelyofiliseerd en werden er affiniteitstesten en calcium-binding proeven op uitgevoerd. De *in vivo* farmacokinetiek en CXCR4-specificiteit van [¹⁸F]AIF-NOTA-DV1-K-(DV3) werden geëvalueerd in gezonde muizen met behulp van μ PET/CT en een *ex vivo* biodistributie studie werd uitgevoerd.

Resultaten: De verschillende modificaties werden succesvol uitgevoerd, met uitzondering van de complexatie van stabiel lanthanum met DOTA-DV1-K-(DV3) en de complexatie van stabiel aluminiumfluoride met NOTA-DV1-K-(DV3). De affiniteitstest en calcium-binding proef toonden aan dat alle geteste constructen inhibitors van CXCR4 waren, weliswaar met verschillende affiniteit en activiteit voor deze receptor. [¹⁸F]AIF-NOTA-DV1-K-(DV3) werd succesvol geproduceerd, maar het HPLC analysesysteem moet nog verder geoptimaliseerd worden. De *in vivo* testen op gezonde muizen toonden gunstige farmacokinetische eigenschappen van [¹⁸F]AIF-NOTA-DV1-K-(DV3), zoals snelle klaring en renale excretie. Bovendien werd opname in de lever (waar er zich CXCR4 expressie bevindt) succesvol geblokt met AMD3100, een CXCR4 antagonist, wat duidt op specificiteit van de tracer voor CXCR4 *in vivo*.

Conclusie: Voorlopige resultaten suggereren dat DV1-K-(DV3) een veelbelovend vectormolecule is voor de ontwikkeling van nieuwe diagnostische en therapeutische radiofarmaceutische preparaten met CXCR4 als doelwit.

Summary

Background: Research has shown that the CXCR4 receptor plays a crucial role in several cancers. Existing CXCR4-targeted imaging and therapy are not optimal. A theranostic approach specifically targeting CXCR4 would be a valuable contribution to the detection and treatment of some cancer types. DV1-K-(DV3), a D-amino acid peptide and CXCR4-antagonist, will be evaluated for the first time as a vector molecule for theranostic radiopharmaceuticals targeting CXCR4.

Objective: In this thesis, the peptide DV1-K-(DV3) was evaluated as a vector molecule for the development of both diagnostic and therapeutic radiopharmaceuticals. Several tests were performed to assess the suitability of DV1-K-(DV3) as a theranostic vector molecule targeting CXCR4.

Methods: Different peptide derivatives were synthesized including a FITC-bound derivative, a RESCA-bound derivative and the corresponding stable aluminium fluoride complex, the NOTA derivative and its corresponding stable aluminium fluoride and gallium complex and a DOTA derivative and its stable lutetium and lanthanum complexes. *In vitro* CXCR4 affinity and calcium-binding assays were performed on the different derivatives. [¹⁸F]AIF-NOTA-DV1-K-(DV3) was synthesized and its pharmacokinetics and *in vivo* CXCR4-specificity was evaluated in healthy mice with μ PET/CT, as well as an *ex vivo* biodistribution.

Results: The envisaged peptide derivatives were obtained, with the exception of lanthanum DOTA-DV1-K-(DV3) and aluminium fluoride NOTA-DV1-K-(DV3). The affinity test and calcium-binding assay showed inhibition of CXCR4 for all the tested constructs, though with varying affinity and/or activity. [¹⁸F]AIF-NOTA-DV1-K-(DV3) was successfully produced, but the quality control system still needs to be optimised. [¹⁸F]AIF-NOTA-DV1-K-(DV3) showed favourable pharmacokinetic properties, such as fast clearance and predominant renal excretion in *in vivo* tests on healthy mice. AMD3100 was able to block [¹⁸F]AIF-NOTA-DV1-K-(DV3) uptake in the liver, which expresses CXCR4, proving *in vivo* CXCR4 specificity of the tracer.

Conclusion: Preliminary results indicate that DV1-K-(DV3) is a suitable vector for CXCR4-targeting diagnostic and therapeutic radiopharmaceuticals.

1. INTRODUCTION

1.1. NUCLEAR MEDICINE

People generally fear radiation, but humanity has found several uses for it since its discovery. In medicine, there are several ways to utilize radioactivity. Most radiation a person encounters during their lifetime is due to natural radioactivity found in our environment; only 12% is artificial radiation and 11% of this is due to medical procedures (Figure 1.1)(1).

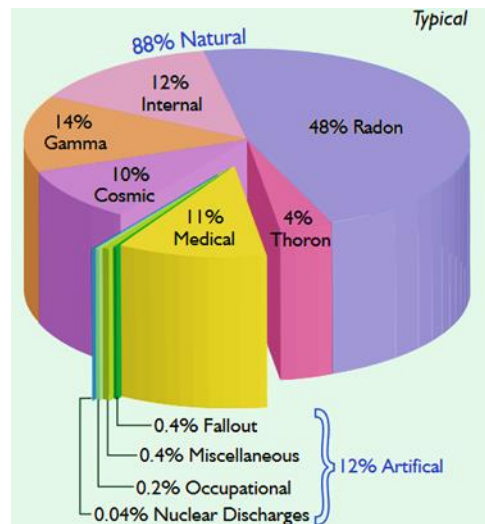


Figure 1.1: Pie chart of the different sources of natural and artificial radiation and their contribution to the total radiation dose. Figure adapted from the World Nuclear Association (1).

Nuclear medicine is a medical specialty that uses small amounts of radioactive compounds (radiopharmaceuticals). These drugs labelled with radioactive isotopes (radioisotopes), are used for medical imaging techniques, like single-photon emission computed tomography (SPECT) or positron emission tomography (PET), and for targeted radionuclide therapy (TRNT)(2). Therefore, they are used in diagnosis, and following up on the efficacy of a treatment or they are used as a treatment. To ensure the radiation burden to healthy tissues is as low as possible and therapeutic radiation selectively targets its goal, radiopharmaceuticals need to have high affinity and high selectivity for their target. These binding properties are achieved by the vector molecule. The vector molecule is the part of the radiopharmaceutical that ensures that the drug accumulates selectively in the target tissue. Several molecules can function as a vector molecule, like small organic molecules, peptides, antibodies, antibody fragments, and proteins. The tissue specificity is therefore determined by the vector binding, not by the decaying isotope. Besides a vector molecule for target accumulation, a radiopharmaceutical also consists out of a radioisotope and a linker (a bifunctional chelator in the case of radiometals) to chemically join the vector molecule and the radioisotope (Figure 1.2)(3).

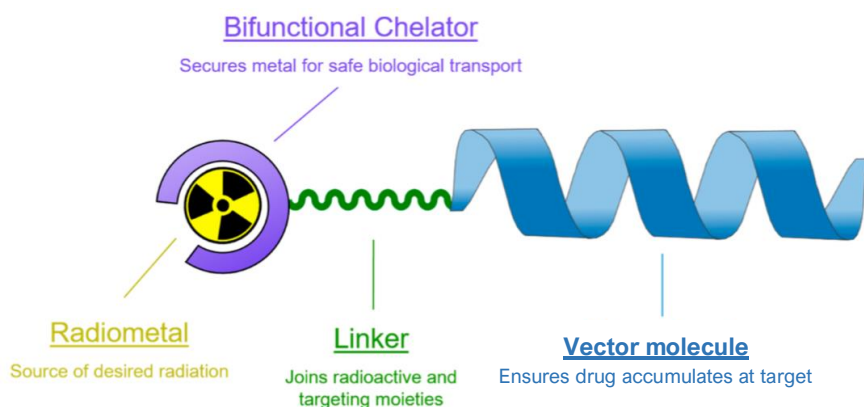


Figure 1.2: Schematic depiction of a radiopharmaceutical, its components and their specific function. Figure adapted from Kostelnik et al. (2019)(4).

Radiotracers are used in such low quantities ((sub)micrograms) that they do not cause a pharmacological effect and thus no direct adverse events (AEs) result from ligand-receptor interactions. This is a major advantage, as (serious) adverse events (SARs) will therefore be less likely to cause the discontinuation of the development of a radiotracer and only limited toxicology studies are required (5). Very few molecules are potent enough to cause a pharmacologic effect at such low quantities, carfentanyl derivatives being an example (6). SARs can also occur due to issues with formulation of the buffer or due to issues with sterility, as radiotracers are injected intravenously.

1.2. RADIONUCLIDES IN NUCLEAR MEDICINE

Several radionuclides are in use in the medical field. The choice of radionuclide for diagnostic or therapeutic application that is used, depends on different factors including the type of radioactive decay the radionuclide undergoes. Some examples of the most commonly used radionuclides and their important characteristics can be found in Table 1.1.

Unstable nuclei decay through emission of radiation to reach a more stable form (7). Nuclear instability is caused by an imbalance between the number of protons and neutrons in a nucleus. Protons usually experience electrostatic repulsion to such an extent that they repel each other. In the nucleus, the electrostatic repulsion is dominated by the strength of the nuclear force between nucleons (protons and neutrons), which is a short-range but very strong force. The higher the atomic number, the more neutrons (relative to the number of protons) are needed to keep the nucleus stable (8).

Table 1.1: Radionuclides used in nuclear medicine for SPECT and PET imaging and for radiotherapy. EC stands for electron capture and IT stands for isomeric transition.

	Isotope	Half-life	Decay type	E (keV)	Production
SPECT (3)	^{99m} Tc	6.06 hours	IT (89%)	γ: 140	⁹⁹ Mo/ ^{99m} Tc generator
	¹¹¹ In	2.83 days	EC (100%)	γ: 245	Cyclotron ¹¹² Cd(p,2n) ^{111m,g} In
	⁶⁷ Ga	3.26 days	EC (100%)	γ: 93	Cyclotron ⁶⁷ Zn(p,n) ⁶⁷ Ga
PET (3)	¹⁵ O	2.0 min	β ⁺ (100%)	β ⁺ _{max} : 1732	¹⁴ N(d,n) ¹⁵ O
	¹¹ C	20.4 min	β ⁺ (100%)	β ⁺ _{max} : 960	Cyclotron ¹⁴ N(p,α) ¹¹ C
	⁶⁸ Ga	67.6 min	β ⁺ (88.9%) EC (11.1%)	β ⁺ _{max} : 1899 γ: 227-2821	⁶⁸ Ge/ ⁶⁸ Ga generator
	¹⁸ F	109.8 min	β ⁺ (97%) EC (3%)	β ⁺ _{max} : 634	Cyclotron ¹⁸ O(p,n) ¹⁸ F
	⁸⁹ Zr	3.3 days	β ⁺ (23%) EC (77%)	β ⁺ _{max} : 902 γ: 909	⁸⁹ Y(p,n) ⁸⁹ Zr
Therapy	²¹¹ At (9)	7.21 hours	α (42%) → EC EC (58%) → α	α: 586 (10)	Cyclotron ²⁰⁹ Bi(α,2n) ²¹¹ At
	⁹⁰ Y (11)	2.67 days	β ⁻ (100%)	β ⁻ : 934	⁹⁰ Sr/ ⁹⁰ Y generator
	¹⁷⁷ Lu (3)	6.65 days	β ⁻ (100%)	β ⁻ _{max} : 497 (10)	Nuclear reactor ¹⁷⁶ Lu(n,γ) ¹⁷⁷ Lu
	²²⁵ Ac (12)	10 days	α (100%)	α: 6000	²²⁹ Th/ ²²⁵ Ac generator Cyclotron ²²⁶ Ra(p,2n) ²²⁵ Ac

The four most important types of radiation are: α-, β⁻, β⁺, and γ- radiation (7). β-particles can have a range of energies with a maximal energy depending on the radionuclide (see Table 1.1), unlike α-particles which are mono-energetic. This range of β-energies will result in different penetration depth of the β-particles that result from the β-decay of a given radionuclide. In general, the higher the energy, the deeper the particles are able to penetrate (13).

1.2.1. Single photon emission computed tomography (SPECT)

SPECT is a nuclear medicine tomographic imaging technique that uses the detection of γ -rays to reconstruct 3D images that correspond to the local concentration of the radionuclide throughout the body. The SPECT radionuclide emits a γ -ray due to transitions from excited nuclear energy levels following decay (14). Collimation (narrow γ -ray filtering) is necessary to select perpendicular radiation in order to allow the construction of sharp images. Ideally, SPECT radioisotopes emit γ -rays with an energy of about 100-250 keV because of easier filtration by collimators and more efficient detection by the SPECT detectors. Technetium-99m (^{99m}Tc) is the most clinically used radioisotope for SPECT scans (4).

1.2.2. Positron emission tomography (PET)

PET is a non-invasive translational and functional imaging technique. It is called a functional (or physiological) imaging technique because the body's molecular changes in absorption, blood flow (distribution), metabolism, and local chemical composition can be quantified. The anatomical integrity of organs and the physiological response of cells can be studied (15).

The emitted positrons resulting from β^+ -decay travel a short distance in the body (the shorter the distance, the higher the resolution (16)) and collide with electrons of the surrounding tissue. When this collision happens, annihilation takes place: the mass of both the positron and the electron is converted to high-energy photons. These 511 keV-photons (γ -rays) travel in opposite directions and are detected by γ -ray detectors of the PET camera (Figure 1.3)(17).

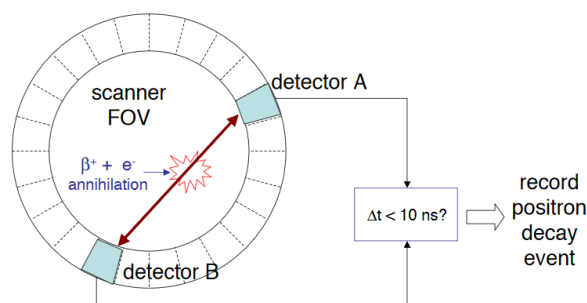
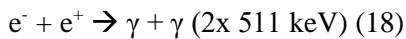


Figure 1.3: PET scanner detection mechanism. A positron is emitted from the radionuclide and collides with an electron. The antimatter-matter collision causes annihilation and two coinciding γ -rays (180° apart) are emitted. These γ -rays are detected by the PET scanner, a computer program calculates where the annihilation took place. FOV stands for field of view. Figure from Courses.Washington.edu (17).

PET radionuclides with a relatively short half-life (e.g. ^{18}F) are mostly used in combination with vector molecules that have fast pharmacokinetic (PK) properties such as small organic molecules and peptides.

Radionuclides with a longer half-life (e.g. ^{89}Zr) are used in combination with vector molecules that have slower PK properties such as antibodies (11).

1.2.3. Advantages of PET over SPECT

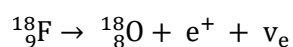
When comparing PET and SPECT, the sensitivity and spatial resolution of PET are superior to those of SPECT, as two coinciding γ -rays are detected, which gives more radiation event localization information. SPECT is more difficult to quantify than PET, as the SPECT camera continuously rotates around the body while the image changes because of the continuous radioactive decay (14). Nonetheless, as mentioned before, nowadays SPECT is still used more frequently than PET because of several reasons (14). SPECT scanners are less expensive than PET scanners (4), $^{99\text{m}}\text{Tc}$ -based SPECT radiotracers are also less costly and more easily available ($^{99}\text{Mo}/^{99\text{m}}\text{Tc}$ generator) than PET radiotracers, for which a cyclotron is generally required (19).

Both PET and SPECT lack anatomical perspective, therefore they are often combined with CT-scans for a more complete depiction of the body's anatomy and its processes (4).

1.2.4. Fluorine-18 and gallium-68; the most used PET radionuclides in clinical practice

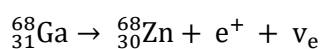
1.2.4.1. Fluorine-18

Fluorine-18 (^{18}F) is a radioactive isotope of the halogen fluorine. It is an artificial isotope with nine protons and nine neutrons. Fluorine-18 is made using a cyclotron starting from oxygen-18 enriched water. Its half-life is 109.8 min and it decays primarily (97%) via β^+ -decay to the stable isotope oxygen-18 by converting a proton into a neutron with emission of a neutrino and a positron (20–22), with a maximum β^+ -energy of 634 keV (3). The remaining 3% decays to oxygen-18 via electron capture (EC)(22).



1.2.4.2. Gallium-68

Gallium-68 (^{68}Ga) is a radioactive isotope of the metal gallium. It has a half-life of 67.6 min and it decays primarily (89%) via β^+ -decay to the stable ground state zinc-68 with a maximum β^+ -energy is 1899 keV. The remaining fraction (11%) decays through EC (3).



Gallium-68 can be produced using a cyclotron or through 'milking' of a germanium-68/gallium-68 generator, in which germanium-68 ($t^{1/2}$ 271 days) decays to gallium-68 (16).

1.2.4.3. Fluorine-18 vs gallium-68

In PET imaging, fluorine-18 is a beloved radioisotope and often preferred to gallium-68 for several reasons. First, fluorine-18 can be produced in high quantities and has a half-life that is sufficiently long to be transported to other hospitals that don't have a cyclotron, yet brief enough to limit the radiation burden for the patient (23). In contrast, gallium-68 has a shorter half-life and a limited batch activity due to the requirement of a generator for its production, making it less suitable for transport to other hospitals (16). Further, germanium-68/gallium-68 generators are expensive but are useful if only small batches are required (3-4 patient doses). An elaborate quality control has to be performed for each batch of a PET tracer, making gallium-68 tracers less cost efficient in terms of manhours per number of patient doses. An advantage of the radiometal gallium is that its chelation can be performed quickly and with high efficiency in aqueous medium, which is an advantage in radiolabelling peptides and proteins. Fluorine-18 usually requires organic synthesis methods proceeding with limited yields and require organic solvents, making it less suitable for direct radiolabelling of peptides and proteins.

Finally, fluorine-18 has a relatively low max positron energy (634 keV), which allows for a higher resolution compared to gallium-68 in a preclinical setting as the emitted positron has a lower penetration depth in tissue prior to annihilation (11).

1.2.5. Therapeutic radionuclides

Therapeutic radiopharmaceuticals have different ways to affect tumours. The type of effect is also determined by the type of radiation that is emitted (α , β^- or Auger electrons). There are three main ways for radiation to cause damage to cells: self-irradiation, crossfire irradiation, and the bystander effect (Figure 1.4)(24).

Self-irradiation occurs when cell death is induced by damage to DNA, the cell membrane, death receptors and/or dysfunctional mitochondria. This can be caused by direct interaction of the radiation with DNA or by interaction of ionizing radiation with water molecules (radiolysis), causing the formation of highly reactive free radicals that can attack essential cellular components (24). Direct interaction of β^- -radiation with DNA generally causes single DNA strand breaks, due to a low (0.2 keV/ μm) linear energy transfer (LET). Auger electrons (intermediate LET of 4-26 keV/ μm) and α -radiation (high LET of 50-230 keV/ μm) generally cause double strand breaks, which are more difficult to repair than single strand breaks (24). Auger electrons have a close range of effectiveness (24), which means they have to bind in close proximity to the target, e.g. DNA, to be effective (25).

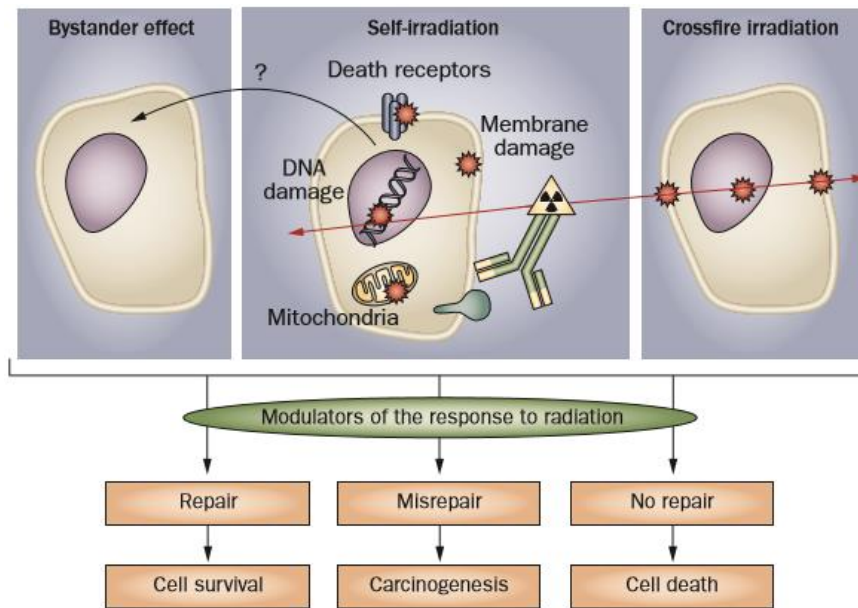


Figure 1.4: Types of effect ionising radiation can have. Bystander effect, self-irradiation and crossfire irradiation can be caused by the radionuclide. Figure from Pouget et al. (2011)(24).

Crossfire irradiation is the second manner in which radiation can damage cells. Crossfire irradiation occurs when a therapeutic radiopharmaceutical binds the target cell, but the depth of the penetration of the radiation is deeper than one cell. This only occurs with β -particles (0.05-12 mm, or a maximum of one hundred cells (24,26)) or α -particles (50-100 μm or multiple cells), as Auger electrons cannot penetrate more than one cell (1-10 nm)(24,26)(Figure 1.5). Using β -radiation, one can even irradiate the whole tumour, even if the target expression is not homogeneous within the tumor, due to the effect of crossfire irradiation (24).

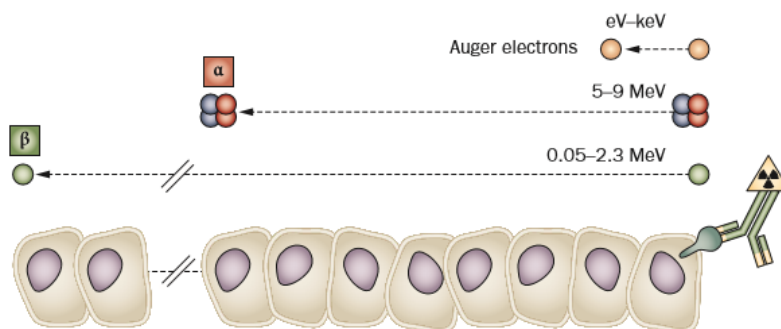
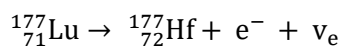


Figure 1.5: The different kinds of particles emitted from decaying radionuclides penetrate cells to a different extent. Auger electrons can penetrate only a single cell, α -particles can penetrate multiple cells and β -particles can penetrate a maximum of one hundred cells. These particles all have a different energy, which ranges from a few eV for Auger electrons to 9 MeV for α -particles. Figure from Pouget et al. (2011)(24).

The last way in which radiation damages cells is due to the bystander effect: apoptosis of one cell results in secretion of signalling molecules that stimulate neighbouring cells to also start programmed cell death cascades (24).

1.2.5.1. Lutetium-177

Lutetium-177 (^{177}Lu) is a radioactive isotope of lutetium, a lanthanide. It is an artificial isotope with 71 protons and 106 neutrons. Lutetium-177 is mostly obtained from radioactive decay of ytterbium-177. Its half-life is about 6.6 days and it decays via β^- -decay to the stable isotope hafnium-177 with emission of an electron and a neutrino (27,28) with a maximum β^- -energy of 497 keV (10).



1.2.5.2. Actinium-225

Actinium-225 (^{225}Ac) is a radioactive isotope of actinium, an actinide. It is an artificial isotope with 71 protons and 106 neutrons. Actinium-225 is obtained from a radium-226/actinium-225 generator or using a cyclotron by deuterium bombardment of radium-226 (29,30).



Its half-life is 10 days and it decays via an α -decay chain to the stable isotope bismuth-209. One of the main advantages of using the actinium-225 isotope for alpha-therapy, is the emission of four alpha particles per actinium-225 atom (12,31), with an α -energy of 6000 keV (12).

A remark has to be made that while actinium itself does not cause a lot of collateral damage, the daughter isotopes might. This is due to the recoil effect, in which the high recoil-energy of the radioactive decay can cause the daughter isotope to detach from the chelator. This recoil-energy is in most cases at least 100 keV, more than 1000 times larger than the chemical bond energy. This simply means that chemical bond rupture between the radionuclide daughter and chelator will always occur subsequent to alpha decay. These daughter isotopes can cause collateral damage, as they are no longer bound to the vector (32) and are therefore free to circulate and potentially accumulate in off-target tissues (e.g. in bone marrow, kidneys) causing radiation damage in healthy tissues.

As the element of actinium only has unstable radioactive isotopes, tests with stable actinium are not possible. Therefore, lanthanum (La) is used as a substitute. It is a metal that has similar properties to actinium (33).

1.3. THERANOSTICS

In theranostics, two similar radiopharmaceuticals with similar PK (distribution, metabolism, elimination) properties are used for diagnosis, therapy and monitoring of the treatment (Figure 1.2). The diagnostic and therapeutic radiopharmaceuticals differ only in terms of the radioisotope that was used (and sometimes also in terms of the chelator that was used). The name theranostic is derived from the

words ‘therapeutic’ and ‘diagnostic’. This approach has been called a game changer for medicine, as it offers an opportunity to save time and money, because only one vector molecule needs to be developed (34). Its biggest advantage is that individual patients can be assessed through PET imaging to investigate whether (a systemic) treatment of all the lesions with the accompanying therapeutic radiopharmaceutical is an option. This is an advantage compared to external beam radiation, which can only be used for primary and large tumours but not for metastatic disease (35).

An important remark that has to be made is that TRNT is generally not a first line therapy for cancer patients. Treatments like surgery, external radiation, and chemotherapy are often attempted first. TRNT is primarily used for systemic treatment of patients that have limited response towards conventional therapies (36) or for patients with distant metastasis. Therapies like surgery, chemotherapy and TRNT are complimentary to one another; for each patient an assessment is made which treatment would be the best option for them in a personalised medicine approach.

An issue with β^- -therapy is that the tumour parenchyma is generally subjected to hypoxic conditions. As the formation of reactive oxygen species is one of the main drivers of the killing effect of radiopharmaceuticals using β^- -radioisotopes, this hypoxic environment is detrimental to the capacity of these radiopharmaceuticals to cause maximum damage. Currently, multi-step pre-TRNT is used to attempt to by-pass this issue (37). When patients do not respond to β^- -therapy due to hypoxic tumours, α -therapy can still be an option, as α -particles mainly cause direct DNA damage and therapeutic efficiency is independent from oxygenation status.

1.4. CHEMOKINE RECEPTOR CXCR4

1.4.1. Chemokines and chemokine receptors

Chemokines, also known as chemotactic cytokines, are small proteins that are secreted by the cell. They are defined by those cysteine residues that are structurally important and put into a subfamily according to their cysteine motif. The subfamilies are the CC, CXC, CX₃C and XC chemokines (38,39).

Chemokines signal through G protein-coupled hepta-helical chemokine receptors on the cell surface and are best known to stimulate the migration of cells, e.g. leukocytes. Therefore, chemokines have a key role in the development, working, and homeostasis of our immune system. Additionally, they play a role in inflammation and involvement of chemokines can be found in all protective and destructive immune and inflammatory reactions (38).

1.4.2. CXC chemokine receptor type 4

The CXC chemokine receptor type 4 (CXCR4)(Figure 1.6), also known as fusin or CD184 (cluster of differentiation 184), is a seven transmembrane G protein-coupled receptor and is encoded by the CXCR4 gene (39). CXCR4 is an α -chemokine receptor that is specific for stromal-derived-factor-1 (SDF-1 α or CXCL12)(39), which was long thought to be its only endogenous ligand (40,41). CXCL12 is a chemokine with intrinsic and potent chemotactic activity for lymphocytes. The CXCR4 receptor is omnipresent in the human body from embryonic development through adulthood.

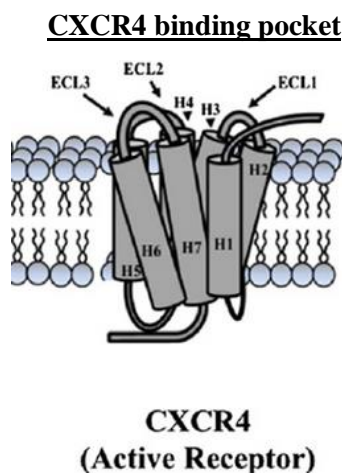


Figure 1.6: The CXCR4 receptor is depicted as an active receptor with the SDF-1 α binding to the CXCR4 binding pocket. ECL stands for extracellular loop and H stands for α -helix. Figure adapted from The Liotta research group (42).

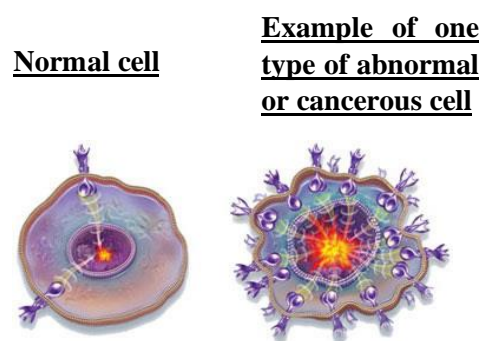


Figure 1.7: Normal cells (left image) only have a few receptors that are expressed in homeostatic conditions. Abnormal or cancerous cells (right image) often have an overexpression of one or more receptors. Figure adapted from Suzuka et al. (2017)(74).

High-expression levels are specially found in endothelial cells and in the hematopoietic system (39): expression occurs in B cells, monocytes/macrophages, neutrophils, T cells, basophils, eosinophils, mast cells and dendritic cells. An overexpression of the receptor can be found in multiple tumours (Figure 1.7).

Under homeostatic conditions, CXCL12 regulates the movement of CXCR4-positive leukocytes and the proliferation and migration of hematopoietic stem cells (42). Furthermore, CXCR4 also plays a critical role as the coreceptor for HIV-1 entry into CD4-expressing lymphocytes (43)(Figure 1.8). It is also thought to stimulate leucocyte recruitment to the damaged myocardium after myocardial infarcts (44) and plays a role in autoimmune diseases like rheumatoid arthritis (42). CXCR4 overexpressing cells move towards tissues with high CXCL12 expression, which causes metastases. Therefore, both CXCR4 and CXCL12 are indicators of a poor survival prognosis in several cancers (42). Additionally, the CXCR4-CXCL12 axis plays a role in several cancer tumour-growth supporting functions (39,42,45): transcription of pro-survival genes in the primary tumor microenvironment; expression of cytokines,

both pro-angiogenic and pro-vasculogenic, promoting access to the systemic circulation of CXCR4-positive cancer cells and promoting tumour progression; immunosuppressive and chemo-resistant adhesion to and migration underneath stroma that is tumour-associated (42). Therefore, several antagonist (small molecules like AMD3100, peptidic molecules like CPCCR4-2 and anti-CXCR4 antibodies like Ulocuplumap) have been developed in an effort to try and disrupt the CXCR4-CXCL12 axis (39).

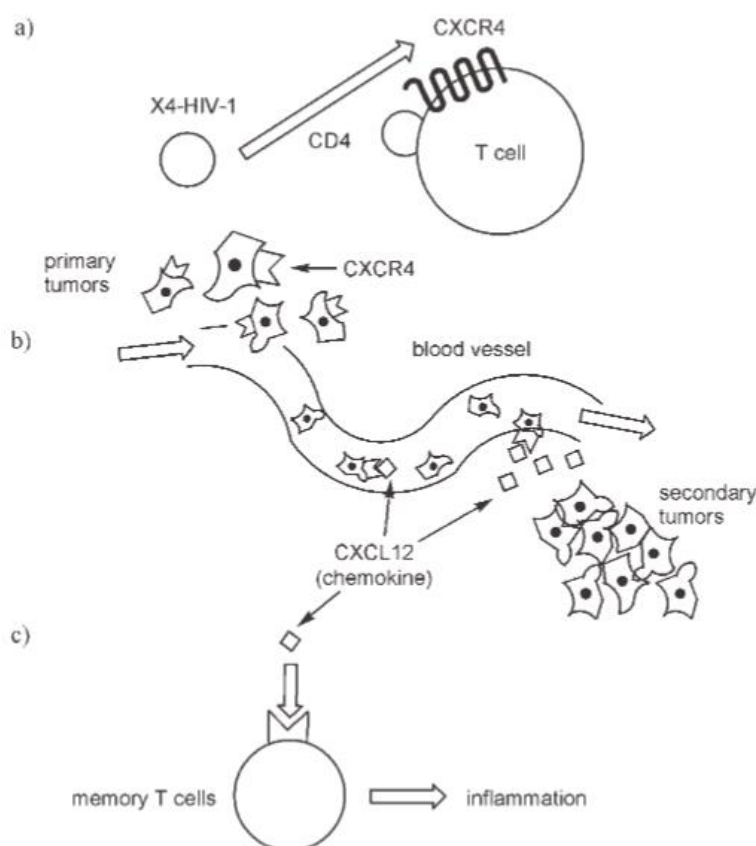


Figure 1.8: Overview of the main pathologies in which the CXCR4 receptor and CXCL12 play an important role. (a) Infection with HIV-1; (b) Cancer and cancer metastasis; (c) Rheumatoid arthritis (RA). Figure from Tsutsumi et al. (2007)(46).

1.5. CURRENT RADIOPHARMACEUTICALS FOR THE CXCR4 RECEPTOR

1.5.1. Radiotracers

Currently, there are some radiotracers available for imaging of CXCR4 receptor expression e.g. in tumour cells. Several classes of vector molecules for CXCR4-antagonists have been developed: cyclams (small molecules) like AMD3100 and AMD11070, peptidic molecules based on the peptidomimetic T140 (a derivative of SDF-1 α (47)) like Ga-NOTA-NFB and small cyclic pentapeptides based on FC131 like Pentixafor and Pentixather.

Some of them were tested in a clinical setting with patients, like [^{64}Cu]Cu-AMD3100 (bicyclam derivative), [^{68}Ga]Ga-NOTA-NFB (T410 derivative) and [^{68}Ga]Ga-Pentixafor (cyclic pentapeptide)(Figure 1.9). All of them have their own advantages and limitations. Studies showed that the bicyclam derivatives and the T140 analogues had a high CXCR4 unrelated splenic and liver uptake in mice and in humans (39). High uptake in these organs makes a tracer unsuitable for high contrast clinical imaging of the expression of the CXCR4 receptor (39). The entire abdomen would have a high activity which would make it difficult if not impossible to detect tumours in this region. Their high uptake in the spleen and liver are likely due to the lipophilic nature of the molecules.

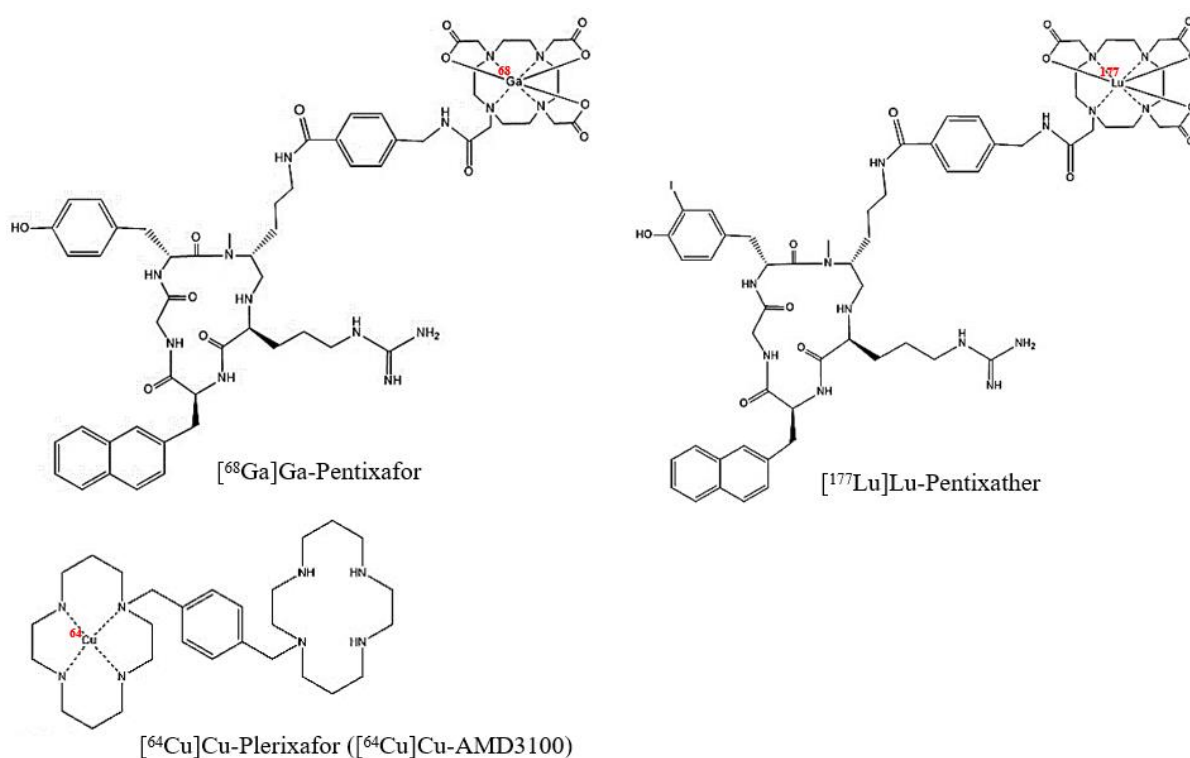


Figure 1.9: Chemical structures of the CXCR4 radiotracers [^{68}Ga]Ga-Pentixafor, [^{64}Cu]Cu-Plerixafor and the therapeutic radiopharmaceutical [^{177}Lu]Lu-Pentixather.

1.5.2. [^{68}Ga]Ga-Pentixafor

[^{68}Ga]Ga-Pentixafor is a tracer that has been developed and used in a clinical setting, with a high affinity for the CXCR4 receptor (half-maximal inhibitory concentration (IC_{50}) value $^{\text{nat}}\text{Ga}$ -Pentixafor: 24.8 ± 2.5 nM), rapid excretion through the kidneys and a high selectivity for human CXCR4. [^{68}Ga]Ga-Pentixafor provides high-contrast PET images of the tissues that express the CXCR4 receptor (48) and is therefore currently the only CXCR4 tracer that is used broadly in a clinical setting (39). Despite this, the use of gallium-68 as the radioisotope has several disadvantages (see chapter 1.2.4.3.). Therefore, finding a fluorine-18 tracer would be a valuable discovery.

To this day, no fluorine-18 tracer is available for the imaging of the CXCR4 receptor in humans. Several attempts have been made to modify the existing radiopharmaceuticals to allow fluorine-18 labelling, but these efforts have yet to yield good results. Attempts to make a fluorine-18 derivative of [^{68}Ga]Ga-Pentixafor have resulted in a loss of affinity for CXCR4 (e.g. $\text{IC}_{50}^{\text{natF-AIF-NOTA-Pentixafor}}$: 220 ± 57 nM;)(49) and a decrease of the metabolic stability (50). A therapeutic counterpart to Pentixafor, using the therapeutic radiometals ^{177}Lu or ^{90}Y were also not successful due to loss of affinity (e.g. $\text{IC}_{50}^{\text{natY}^{3+}\text{-Pentixafor}}$: 40.8 ± 27 nM; e.g. $\text{IC}_{50}^{\text{natLu}^{3+}\text{-Pentixafor}}$: 40.9 ± 12 nM). Indeed, replacing gallium with lutetium caused the affinity to decrease by half (49).

1.5.3. [^{177}Lu]Lu-Pentixather

Due to the inability to modify the Pentixafor scaffold to obtain a fluorine-18 tracer or a therapeutic radiopharmaceutical, a different scaffold had to be designed. Therefore, the Pentixather scaffold was created by iodinating the Pentixafor scaffold on tyrosine-1 (53). The affinity of [^{177}Lu]Lu-Pentixather (Figure 1.9) for the CXCR4 receptor is high ($\text{IC}_{50}^{\text{natLu-Pentixather}}$: 14.6 ± 1.0 nM)(53). However, these modifications made the molecule more lipophilic (increase of the logP from -2.9 to -1.76 (52)) by more than one order of magnitude) and profoundly changed its PK properties (49,51). [^{177}Lu]Lu-Pentixather is primarily cleared via the liver, while [^{68}Ga]Ga-Pentixafor mainly has renal clearance. The spleen also shows high uptake. Due to the fact that the PK profile of [^{68}Ga]Ga-Pentixafor does not match the PK profile of [^{177}Lu]Lu-Pentixather (Figure 1.10), the theranostic approach is undermined.

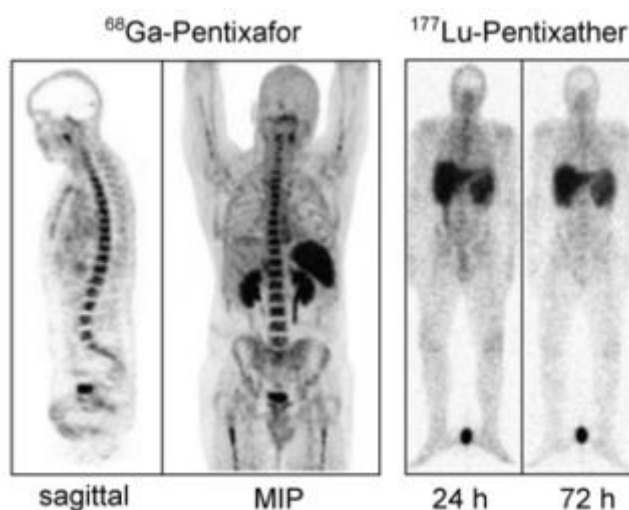


Figure 1.10: PET imaging and planar whole-body scintigraphic images of [^{68}Ga]Ga-Pentixafor, 24 hours and 72 hours p.i. of [^{177}Lu]Lu-Pentixather (200 MBq) in a patient. Figure from Habringer et al. (2018)(53).

[¹⁷⁷Lu]Lu-Pentixather is mostly used as therapy for various CXCR4-overexpressing tumours and especially before hematopoietic stem cell transplantation in patients suffering from lymphoproliferative or myeloid malignancies, as CXCR4 is also expressed in bone marrow (54)(Figure 1.10). As a stem cell transplantation is always necessary after treatment of lymphoproliferative and myeloid malignancies, the bone marrow toxicity of the anti-CXCR4 therapy is not an issue and can even be an advantage. When treating solid tumours, the bone marrow toxicity of this treatment is a reason to choose another therapy.

1.6. DV1-K-(DV3) PEPTIDE AS CXCR4 ANTAGONIST

The human herpesvirus-8 (HPV-8) encodes a viral chemokine, macrophage inflammatory protein-II (vMIP-II), which has a high affinity for CXCR4 with an IC₅₀ of 3.0 nM (55). As the CXCR4 receptor plays a crucial role in cellular entrance of HIV-1, CXCR4 antagonists are being evaluated for HIV treatment. vMIP-II's potency was discovered in an effort to find an anti-HIV drug that would block the CXCR4 receptor (56). vMIP-II can inhibit the calcium responses that the endogenous ligand (CXCL12) induces. Furthermore, it can also inhibit cancer cell migration *in vitro* (55). Xu *et al.* (2013) demonstrated that it was the N-terminus of the vMIP-II protein that contained the essential amino acid (AA) sequence (21 AA) to bind the CXCR4 receptor and they found remarkable stereochemical flexibility. This essential AA sequence was called V1 and a D-AA analogue was constructed, which was called DV1 (57). Another peptide was synthesized, DV3, which consists out of the first 10 subsequent AA residues of DV1 (Table 1.2). The affinity of both peptides was determined (IC₅₀ DV1: 236 nM; IC₅₀ DV3: 440 nM)(56). Next, a bivalent peptide (DV1-K-(DV3) or HC4319) was constructed by conjugating the DV1 sequence to the DV3 sequence through an added C-terminal D-lysine ε-moiety. This DV1-K-(DV3) bivalent peptide has the highest affinity for the CXCR4 receptor (IC₅₀ 4.0 nM), higher than either DV1 or DV3. This higher affinity of the bivalent peptide might be caused by the fact that the CXCR4 receptor can be expressed as a dimer (56) or by the fact that the dimer can bind both the major and the minor subpocket of CXCR4 (58). Nevertheless, it is unusual that a peptide consisting of D-AAAs still has a high affinity for the target receptor. The D-conformation of the AAAs was chosen, as this would allow the peptide to have a higher metabolic stability through slower degradation, because D-AAAs are not recognized by the proteolytic enzymes of the human body (56). It was also demonstrated by Mao *et al.* (2018) that DV1-K-(DV3) does not bind CXCR7 (55).

Table 1.2: Amino acid structure of vMIP-II, V1, V3, DV1, DV3 and DV1-K-(DV3). In DV1-K-(DV3), DV1 is coupled to DV3 via the ϵ -amino moiety of a leucine that was added. The IC_{50} values were characterized using the monoclonal antibody 12G5 (55).

Peptide	Amino acid sequence	Conformation of amino acids	IC_{50} (nM) (56)
vMIP-II	H ₂ N-LGASWHRPDKCCLGYQKRPLPQVL LSSWYPTSQLCSKPGVIFLTKRGRQ VCADKSKDWVKKLMQQLPVTAR-COOH	L	3
V1	H ₂ N-LGASWHRPDKCCLGYQKRPLP-COOH	L	456
V3	H ₂ N-LGASWHRPDK-COOH	L	> 10.000 (59)
DV1	H ₂ N-LGASWHRPDKCCLGYQKRPLP-COOH	D	236
DV3	H ₂ N-LGASWHRPDK-COOH	D	440
DV1-K- (DV3) (bivalent peptide)	H ₂ N-LGASWHRPDKCCLGYQKRPLPK-COOH H ₂ N-LGASWHRPDK	D	~ 4

2. AIMS/OBJECTIVES

CXCR4 is an important target in myocardial infarct, HIV and oncology research, both for diagnostic and therapeutic applications. Many cancers are found to overexpress the CXCR4 receptor. The current radiopharmaceuticals for CXCR4 either have a high splenic and liver uptake and are therefore unsuitable for high contrast clinical imaging of the expression of CXCR4, or they use gallium-68 (e.g. [⁶⁸Ga]Ga-Pentixafor) of which production capacity is limited due to high cost of the germanium-68/gallium-68 generator, low production yield, and its relatively short half-life. Attempts to make a fluorine-18 derivative of [⁶⁸Ga]Ga-Pentixafor have failed, due to loss of affinity, and no other promising fluorine-18 tracer is available on the market. A second issue is the difference in PK profile of the diagnostic radiotracer [⁶⁸Ga]Ga-Pentixafor and the therapeutic radiopharmaceutical [¹⁷⁷Lu]Lu-Pentixather, which undermines the theranostic approach.

Therefore, the aim of this project is to develop both diagnostic and therapeutic radiopharmaceuticals targeting CXCR4 expressing malignancies. A new vector molecule, DV1-K-(DV3), will be used to develop a fluorine-18 CXCR4 tracer and its accompanying therapeutic radiopharmaceutical. The use of the same vector molecule is expected to result in a similar PK profile for both the diagnostic and therapeutic radiopharmaceutical. Further, as the vector molecule is a peptide, the use of the therapeutic radiopharmaceutical can be considered as peptide receptor radionuclide therapy (PRRT)(60). DV1-K-(DV3) is expected to have a high affinity, high selectivity and moreover, a high predicted *in vivo* stability due to its D-AAAs composition. The final aim of this project is to translate this new class of radiopharmaceuticals into the clinic. The aim of this thesis is to start with fundamental research (development of new CXCR4 targeted radiopharmaceuticals) and conduct part of the preclinical evaluation (Figures 2.1 and 2.2).

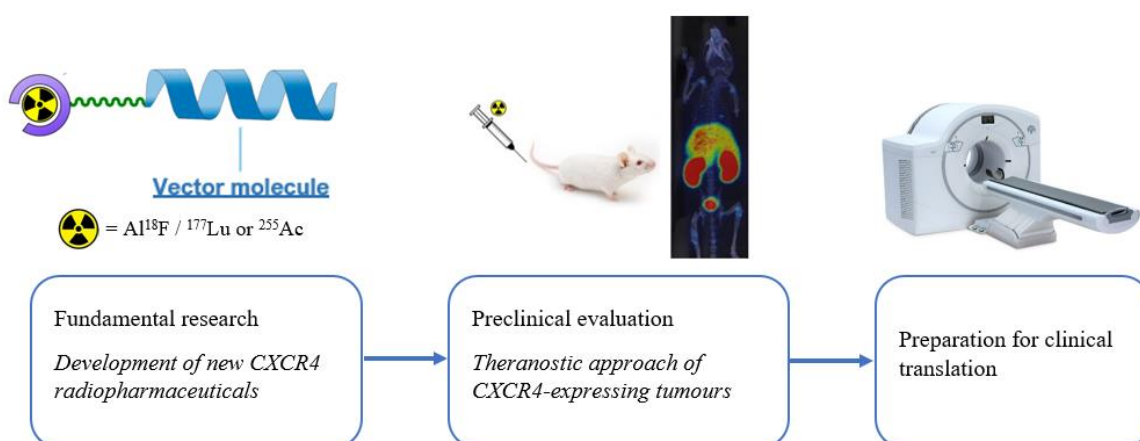


Figure 2.1: Different parts of the project: fundamental research and preclinical evaluation in preparation of future clinical translation. Figures adapted from Kostelnik et al. (2019)(4) and from MinFound Medical Systems (61).

In the fundamental research part, three different chelators will be conjugated to the DV1-K-(DV3) peptide. These chelators are 1,4,7-triazacyclononane-1,4,7-triacetic acid (NOTA), restrained complexing agent (RESCA) and 1,4,7,10-tetraazacyclododecane-1,4,7,10-tetraacetic acid (DOTA).

DV1-K-(DV3) will be derivatised with the NOTA-chelator for fluorine-18 tracer development via the Al¹⁸F-method, the RESCA-chelator for fluorine-18 tracer development via the Al¹⁸F-method, the DOTA-chelator for development of ¹⁷⁷Lu- and ²²⁵Ac-labelled radiopharmaceuticals with PRRT as application, and with the fluorescent dye fluorescein isothiocyanate (FITC) isomer I to examine subcellular CXCR4 distribution in tumour tissue. In addition, both the NOTA and DOTA constructs can also be labelled with the diagnostic radionuclide gallium-68 if required.

Next, the complexes with stable isotopes of the envisaged radionuclides will be synthesised (AlF, Lu, Ga, and La (as stable Ac is not available)) and affinity tests and functionality tests (through a calcium-binding assay) will be performed on CXCR4 expressing Jurkat cells (collaboration with the lab of prof. D. Schols, Rega Institute KU Leuven).

For the preclinical evaluation, radiolabelling of NOTA-DV1-K-(DV3) with [¹⁸F]AlF will be performed and a QC system will be developed. Finally, the PK profile of [¹⁸F]AlF-NOTA-DV1-K-(DV3) will be determined by performing μ PET/CT studies in healthy mice followed by *ex vivo* biodistribution.

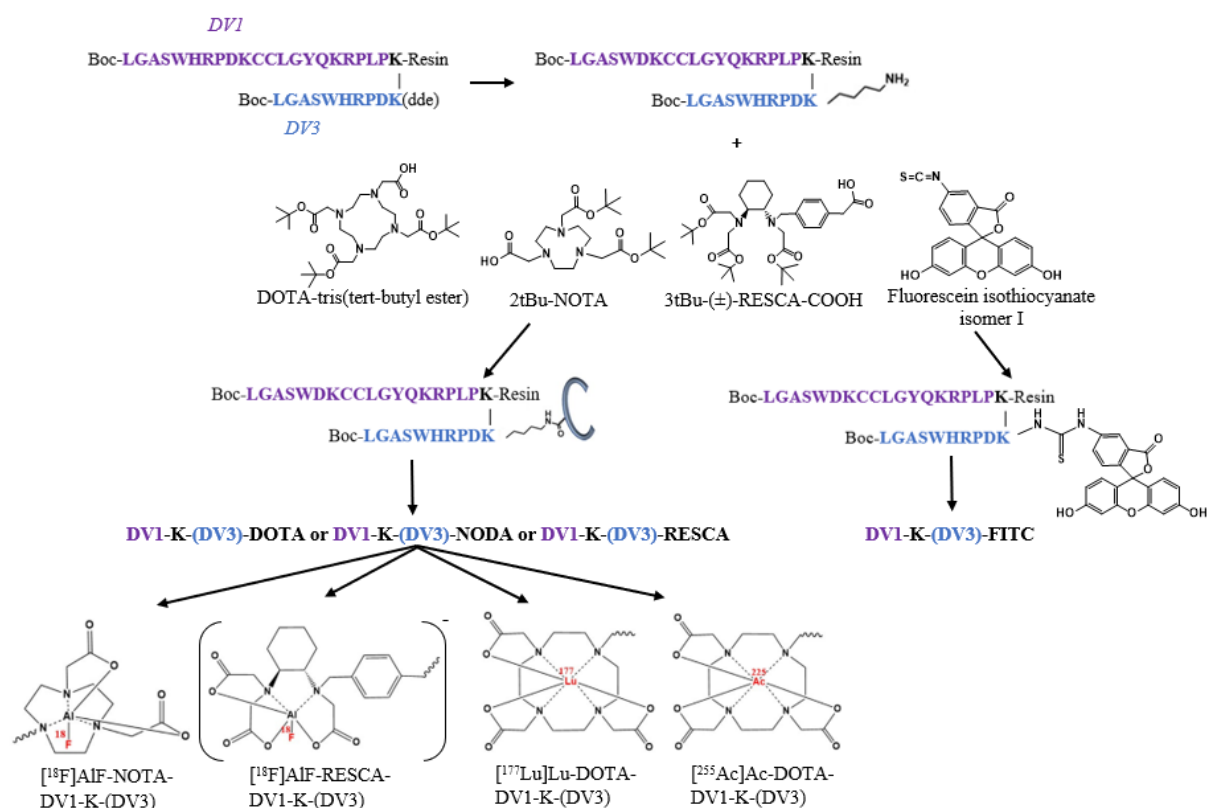


Figure 2.2: Schematic depiction of how all constructs were made. The structures of the used chelators (DOTA, RESCA and NOTA) with their respective radionuclides and with the chelators bound to DV1-K-(DV3) are depicted, as well as the FITC structure and FITC attachment to DV1-K-(DV3).

3. MATERIALS AND METHODS

3.1. MATERIALS

All solvents and reagents were obtained from Acros Organics (Geel, Belgium), CheMatech (Dijon, France), Fagron (Nazareth, Belgium), Fisher Scientific (Doornik, Belgium), Fluka (Bornem, Belgium), Sigma-Aldrich (Bornem, Belgium) and VWR (Leuven, Belgium). DV1, DV3, DV1-K-(DV3), DOTA-DV1-K-(DV3) and NOTA-DV1-K-(DV3) were obtained from Pepmic (Suzhou, China).

The Sep-Pak Plus Light C₁₈ cartridges were obtained from Waters (Asse, Belgium), the Captiva PTFE+GF 0.45 μm filters were obtained from Agilent (Diegem, Belgium), and the Millex-GV 13 mm (0.22 μm) filters were obtained from Merck Millipore (Tullagreen, Ireland). The Intavis 5 mL reaction columns and the Intavis column module filters were obtained from Intavis Bioanalytical Instruments AG (Köln, Germany).

[¹⁸F]Fluoride was made on site using an ¹⁸O(p,n)¹⁸F reaction. 2 mL of 97% enriched [¹⁸O]H₂O (HYOX18 Rotem Industries Beer Sheva, Israel) was irradiated with 18 MeV protons produced in a Cyclone 18/9 cyclotron (Ion Beam Applications, Louvain-la-Neuve, Belgium) in a niobium target. The activity of the radioisotopes was measured using a Radioisotope Calibrator CRC-721 (an ionization chamber-based activity meter)(Capintec; Ramsey, NJ, US). The AllinOne module (Trasis; Ans, Belgium) was used for the radiochemical reactions.

Constructs were lyophilised using a VirTis Freezemobile 12SL Unitop 400SL Freeze dryer (VirTis Company; Gardines, N.Y., US).

Liquid chromatography high resolution mass spectrometry (LC-HRMS) was performed using a Dionex UltiMate 3000 RS UHPLC System (Thermo Fisher Scientific; Sunnyvale, USA), which is coupled in series to a maXis impact ultra-high resolution time-of-flight mass spectrometer (TOF-HRMS) (Bruker; Bremen, Germany) with an orthogonal electrospray ionization (ESI, positive medium mode using HCOOH) interface. An Acquity UPLC C₁₈-column (2.1x50 mm; 1.7 μm), with an Acquity UPLC BEH C₁₈ VanGuard Pre-column (2.1x5 mm; 1.7 μm)(Waters; Massachusetts, USA) were used and coupled in series with a fluorescence-detector. The mobile phase contains H₂O (0.1% HCOOH) and acetonitrile (ACN)(0.1% HCOOH) as the organic modifier. The flow rate was 0.6 mL/min. The elution gradient was the following: 0-2 min: 5% ACN (0.1% HCOOH); 2-8 min: 5% to 95% ACN (0.1% HCOOH); 8-10 min: 95% ACN (0.1% HCOOH); 10-12 min: 95% to 5% ACN (0.1% HCOOH). Analysis of the data was performed using HyStar software and processing of the data was done using Compass DataAnalysis (version 4.1, Bruker). Compass IsotopePattern (version 2.0 Bruker) was used to obtain the calculated monoisotopic mass of the compounds.

The microPET (μPET) scans were obtained using the β-CUBEs and X-CUBE (Molecubes; Gent, Belgium).

The biodistribution studies were performed using an automated 1480 Wizard 3q gamma counter equipped with a 3-inch NaI(Tl) well crystal which was coupled to a multichannel analyser, and mounted in a sample changer (Perkin Elmer; Zaventem, Belgium). Counts were corrected for background radiation, physical decay and counter dead time.

The UV spectrum of FITC was made using the Nanodrop 2000 (Thermo Fisher Scientific; Sunnyvale, USA).

Radiochemical reactions were monitored using an HPLC system, consisting of an Elite LaChrom VWR Hitachi pump L-2130 connected to an Elite LaChrom VWR Hitachi UV detector L-2400 and a NaI scintillation detector, an Alltech Elite On-line Degassing System (Grace Davison Discovery Sciences; Lokeren, Belgium), and a GABI Star acquisition system (Elysia Raytest; Angleur, Belgium).

ChemDraw™ Professional was used to draw the molecular structures.

A BD FACSCanto™ II and BD FACSArray (Becton Dickinson; Erembodegem, Belgium) was used at the Rega institute to perform the flow cytometry experiments. The BD FACSDIVA Software and BD FACSArray System Software (Becton Dickinson; Erembodegem, Belgium) were used as software to analyse the data.

For the calcium mobilisation tests performed at the Rega institute, a FLIPR Tetra high throughput cellular screening system as the fluorescent plate reader for the calcium mobilisation tests, the FLIPR Tetra LED Module 470-495 nm as the light emitting diodes to induce the excitation of the fluorescent Ca²⁺-sensitive dye, the FLIPR Tetra Emission Filter 515-575 nm as the emission filter and a FLIPR Tetra 96 Head as a 96-well pipettor head (Molecular Devices; San Jose, CA, USA) and the Vi-CELL (Beckman Coulter; Suarlée, Belgium) were used as the cell viability analyser. The software used to analyse and visualise the data was the ScreenWorks software (Molecular Devices; San Jose, CA, USA).

3.2. SYNTHESIS AND PURIFICATION OF RESCA-DV1-K-(DV3)

100 mg of DV1-K-(DV3) resin (0.02 mmol, 1 equivalent), without protective groups on the dde groups, was weighed into an Intavis 5 mL reaction column with an Intavis filter for the column to ensure the resin did not fall out of the reaction column. The resin was allowed to swell in 2 mL dichloromethane (DCM) for 10 min at room temperature and under constant shaking. The DCM was removed and 2 mL dimethylformamide (DMF) was added to rinse away the DCM. The DMF was removed after 2 min and 2 mL of fresh DMF was added again. The resin with DMF was continuously shaken. In a vial, a mixture of 38 mg 2-(7-Aza-1H-benzotriazole-1-yl)-1,1,3,3-tetramethyluronium hexafluorophosphate (Hatu) (0.1 mmol, 5 equivalents), 1 mL DMF and 17.5 µL N-Ethyldiisopropylamine (DIPEA)(0.02 mmol, 1 equivalent) and 30 mg of t₃tBu-(±)RESCA-COOH (0.05 mmol, 2.5 equivalents) (Mr 604.37 g/mol) was added. The mixture was shaken for 10 min in a vial at room temperature. In another vial, 0.5 mL of

DMF and 17.5 μ L of DIPEA were added together. The DMF-DIPEA mixture was added to the DV1-K-(DV3) resin. After, the RESCA-mixture was also added to the DV1-K-(DV3) resin. The mixture was allowed to react for two hours at room temperature. Next, the resin was washed 3 times with 2 mL DMF (2 min per washing step). Subsequently, the resin was washed 3 times with 2 mL DCM (2 min per washing step). The resin was dried overnight in a vacuum oven.

The cleavage mixture consisted of 1.85 mL of trifluoroacetic acid (92.5%)(TFA), 0.05 mL of metal-free water (2.5%) and 0.1 mL tri-isopropyl silane (5%)(Tis). The cleavage mixture was added to the resin and allowed to react for two hours at room temperature under constant shaking. The mixture was filtered through the reaction column and collected in a round bottom flask. The reaction column was flushed with 2 mL TFA and it was collected in the same round bottom flask. The solvent was evaporated from the round bottom flask by reduced pressure and an elevated temperature (40°C).

Purification of the synthesized RESCA-DV1-K-(DV3) compound was performed by HPLC. The RESCA-DV1-K-(DV3) was dissolved in 1 mL ACN/water (LC-MS grade) 50/50% v/v.

A gradient of water (0.1% TFA) with ACN (0.1% TFA) as organic modifier was used at a flow rate of 5 mL/min with a Waters XBridge C₁₈ prep column (10x250 mm; 5 μ m). Table 3.1 depicts the gradient that was used. The UV detection wavelength was 220 nm, as the peptide has a maximum absorbance at that wavelength. The peak was collected at about 12 min after the start of the HPLC-run. A sample for LC-MS analysis was taken and the vial was dried overnight in a vacuum oven. After drying, the vial was filled with N₂ gas, covered in aluminium foil and stored in the freezer (-20°C).

Table 3.1: Gradient used for the HPLC purification of RESCA-DV1-K-(DV3). Water (0.1% TFA) was used as the mobile phase, acetonitrile (0.1% TFA) was used as the organic modifier.

	Water (0.1% TFA)	Acetonitrile (0.1% TFA)
0 min	83%	17%
15 min	70%	30%
15-20 min	20%	80%
20-30 min	83%	17%

3.3. FITC-DV1-K-(DV3) SYNTHESIS

For the FITC-DV1-K-(DV3) synthesis, 100 mg of resin-bound DV1-K-(DV3) without protective groups (0.02 mmol, 1 equivalent) was used. The resin was put into an Intavis 5 mL reaction column with an Intavis filter for the column and allowed to swell for 10 min using 2 mL DCM. Next, the DCM was removed and the resin was rinsed twice with 2 mL anhydric DMF (2 min/washing step). In a separate

vial, a solution was made using 2 equivalents (in regards to the peptide) of FITC (16 mg), 1 mL anhydric DMF and 70 μ L DIPEA (2 equivalents). The FITC solution was stirred for 10 min at room temperature and covered in aluminium foil. In another vial a solution of 0.5 mL anhydric DMF and 70 μ L DIPEA (2 equivalents) is made, subsequently added to the resin in the reaction column and shaken for 2 min at room temperature. Next, the FITC-solution is also added to the resin in the reaction column. The reaction column was covered in aluminium foil and shaken for two hours at room temperature. After, the solution was removed from the reaction column and the resin was rinsed three times with 2 mL anhydric DMF (2 min/washing step) and then three times with 2 mL DCM (2 min/washing step). Finally, the resin was dried overnight under reduced pressure, the reaction column was attached to a 0.22 μ m filter to minimize contamination and aluminium foil to reduce the light exposure.

A microcleavage was performed on the FITC-DV1-K-(DV3) construct. A few grains of dried resin were taken and the FITC-DV1-K-(DV3) construct was cleaved from the resin by adding 0.5 mL of a cleavage cocktail. The cleavage cocktail consisted of 92.5% TFA, 2.5% metal-free water and 5% Tis. The cleavage took two hours at room temperature and the solution was also protected from light exposure by using aluminium foil. Next, the content was transferred to a weighed round bottom flask and the original recipient (the reaction column) was rinsed three times with 2 mL TFA (shaken 2 min/step), which was also added to the weighed round bottom flask. The solution was dried using reduced pressure at a temperature of 40°C. After drying, an LC-MS sample was taken.

3.4. LABELLING WITH STABLE ISOTOPES

3.4.1. $^{nat}\text{F}^-$ -AIF-labelling of NODA-MP-NCS

The protocol for the $^{nat}\text{F}^-$ -AIF-labelling of NODA-meta phenyl-isothiocyanate (NODA-MP-NCS) was based on the protocol in the paper of Cleeren *et al.* (2018)(62). A solution was made containing AlCl_3 (2 mL, 0.075 mmol, 3 equivalents in 0.1 M sodium acetate, pH 4.5) and the NODA-MP-NCS (0.025 mmol, 1 equivalent) (Mr 392.47 g/mol). The reaction mixture was allowed to react for two hours at a temperature of 95°C with regular stirring to ensure Al^{3+} -complexation. After cooling, the mixture was loaded onto an activated Sep-Pak Plus Light C_{18} . The vial was rinsed with 2 mL metal-free water and this was loaded onto the activated Sep-Pak Plus Light C_{18} . The cartridge was rinsed two times with water (2 mL) and eluted with 2 mL dry ACN. The solvent was evaporated under reduced pressure. The $\text{Na}[\text{Al}(\text{OH})(\text{NODA})\text{-MP-NCS}]$ was dissolved in 2 mL dry ACN and 0.025 mmol (1 equivalent) of tetraethylammonium fluoride dihydrate (TEAF) was added. The solution was stirred at room temperature during one hour. The solution was dried under reduced pressure. To the residue, 2 mL of metal-free water was added. The obtained solution was loaded onto an activated Sep-Pak Plus Light C_{18} cartridge (Waters), rinsed two times with 2 mL metal-free water and subsequently eluted with 2 mL dry ACN. A sample was taken for LC-MS analysis.

The solvent was once again evaporated under reduced pressure to obtain (\pm)-[N(Et)₄][AlF(NODA)-MP-NCS]. The vial was filled with N₂ gas, covered in aluminium foil and stored in the freezer (-20°C).

3.4.2. ^{nat}Ga³⁺-labelling of NOTA-DV1-K-(DV3)

The protocol for the ^{nat}Ga³⁺-labelling of NOTA-DV1-K-(DV3) was based on the protocol in the paper of Suzuki *et al.* (2019)(63). A solution was made containing Ga(NO₃)₃ (220 μ L, 20 mM in 0.1 M sodium acetate, pH 5, 20 equivalents) and the NOTA-bound peptide without protective groups (1 mg, 1 mM, 1 equivalent) (Mr 3987.58 g/mol). The reaction mixture was allowed to react for 30 min at a temperature of 95°C with regular stirring to ensure Ga³⁺-complexation. After cooling, the mixture was diluted with 2 mL metal-free water and this was loaded onto the activated Sep-Pak Plus Light C₁₈. The vial was rinsed with 1 mL metal-free water and this was also loaded onto the activated Sep-Pak Plus Light C₁₈.

The peptide was eluted with 1 mL absolute ethanol into a vial. An LC-MS sample was taken and the vial was dried overnight in a vacuum oven. After drying, the vial was filled with N₂ gas, covered in aluminium foil and stored in the freezer (-20°C).

3.4.3. ^{nat}Ga³⁺-labelling of DOTA-DV1-K-(DV3)

The protocol for the ^{nat}Ga³⁺-labelling of DOTA-DV1-K-(DV3) was based on the protocol in the paper of Suzuki *et al.* (2019)(63). A solution was made containing Ga(NO₃)₃ (220 μ L, 20 mM in 0.1 M sodium acetate, pH 5, 20 equivalents) and the DOTA-bound peptide (0.9 mg, 1 mM, 1 equivalent) (Mr 4088.69 g/mol). The reaction mixture was allowed to react for 30 min at a temperature of 95°C with regular stirring to ensure Ga³⁺-complexation. After cooling, the mixture was diluted with 2 mL metal-free water and this was loaded onto the activated Sep-Pak Plus Light C₁₈. The vial was rinsed with 1 mL metal-free water and this was also loaded onto the activated Sep-Pak Plus Light C₁₈. The peptide was eluted with 1 mL absolute ethanol into a vial. An LC-MS sample was taken and the vial was dried overnight in a vacuum oven. After drying, the vial was filled with N₂ gas, covered in aluminium foil and stored in the freezer (-20°C).

3.4.4. ^{nat}Lu³⁺-labelling of DOTA-DV1-K-(DV3)

The protocol for the ^{nat}Lu³⁺-labelling of DOTA-DV1-K-(DV3) was also based on the protocol in the paper of Suzuki *et al.* (2019)(63). A solution was made containing LuCl₃ (220 μ L, 20 mM in 0.01 M HCl, 20 equivalents) and the DOTA-bound peptide (0.9 mg, 1 mM, 1 equivalent) (Mr 4088.69 g/mol). The reaction mixture was allowed to react for 30 min at a temperature of 95°C with regular stirring to ensure Lu³⁺-complexation. After cooling, the mixture was diluted with 2 mL metal-free water and loaded onto an activated Sep-Pak Plus Light C₁₈. The vial was rinsed with 1 mL metal-free water and this was loaded onto the activated Sep-Pak Plus Light C₁₈ As well.

The peptide was eluted with 1 mL absolute ethanol into a vial. An LC-MS sample was taken and the vial was dried overnight in a vacuum oven. After drying, the vial was filled with N₂ gas, covered in aluminium foil and stored in the freezer (-20°C).

3.4.5. ^{nat}La³⁺-labelling of DOTA-DV1-K-(DV3)

The protocol for the ^{nat}La³⁺-labelling of DOTA-DV1-K-(DV3) was based on the protocol in the paper of Ucar *et al.* (2019)(64). A solution was made containing LaCl₃ (220 µL, 20 mM in 0.1 M Tris buffer, pH 9, 20 equivalents) and the DOTA-bound peptide (0.9 mg, 1 mM, 1 equivalent)(Mr 4088.69 g/mol). The reaction mixture was allowed to react for 30 min at a temperature of 95°C with regular stirring to ensure La³⁺-complexation. After cooling, the mixture was diluted with 2 mL metal-free water and this was loaded onto the activated Sep-Pak Plus Light C₁₈ As well. The vial was rinsed with 1 mL metal-free water and this was also loaded onto the activated Sep-Pak Plus Light C₁₈.

The peptide was eluted with 1 mL absolute ethanol into a vial. An LC-MS sample was taken and the vial was dried overnight in a vacuum oven. After drying, the vial was filled with N₂ gas, covered in aluminium foil and stored in the freezer (-20°C).

3.5. LYOPHILIZATION

To each of the vials containing the purified RESCA-DV1-K-(DV3), the cold constructs that were synthesized and the FITC-construct, 1 mL metal-free water and 440 µL ACN (LC-MS grade) was added. For optimal solubilization, the vials were put in the sonification machine for 5 min. To ensure a clear solution was obtained, the content of each vial was purified using a Captiva PTFE + GF 0.45 µm filter from Agilent. Again, samples for LC-MS testing were taken. The constructs were subsequently cooled in a freezer (-20°C) for an hour and lyophilized afterwards. Then, the vacuum was broken, the vials were weighed, filled with N₂ gas, covered in aluminium foil and stored in the freezer again (-20°C).

3.6. AFFINITY TESTS

The lab of Dr. Dominique Schols at the Rega institute (lab of virology and chemotherapy) kindly performed the affinity assays according to a previously published assay by Schoofs *et al.* (2018)(65).

Jurkat cells were used for the affinity assay and the calcium-binding assay, as they naturally express CXCR4 in a stable manner. The fact that they are suspension cells makes an affinity assay easier, as there is no need for trypsin to cut them loose (trypsin can also damage the receptors). The lack of CXCR7 expression makes them valuable in specificity testing.

The affinity tests were performed twice. The different peptide-constructs were tested for their inhibitory properties. AMD3100 and AMD11070 were used as reference CXCR4 receptor inhibitors.

The Jurkat cells were washed with a Ca^{2+} -buffer during 5 min and subsequently resuspended ($4 \cdot 10^6$ cells/mL) in a Ca^{2+} -buffer. In a round-bottom 96 well plate, 100 μL compound (DV1-K-(DV3), NOTA-DV1-K-(DV3), AIF-NOTA-DV1-K-(DV3), DOTA-DV1-K-(DV3), Ga-DOTA-DV1-K-(DV3), Lu-DOTA-DV1-K-(DV3) or La-DOTA-DV1-K-(DV3)) and 50 μL of the cell suspension were added. Several concentrations of AMD3100 were tested (ranging from 0.192 to 600 nM) as well as several concentrations of AMD11070 (ranging from 0.04 to 115 nM) and several concentrations of the DV1-K-(DV3) peptide (ranging from 0.0256 to 10.000 nM)(See Figure 3.1). The cells were incubated at room temperature for 15 min in the dark. After, 50 μL of SDF- AF^{647} (25 ng/mL CXCL12 AF^{647} dissolved in assay buffer) was added and allowed to incubate for 30 min at room temperature in the dark. Then, the cells were washed twice with a Ca^{2+} -buffer and centrifuged for 3 min. Finally, the cells were fixed with 200 μL of BD CellFIX 1% and the AF^{647} signal was read by the BD FACSCantoTM II.

AMD3100

600	120	24	4,8	0,96	0,192	nM
-----	-----	----	-----	------	-------	----

AMD11070

115	23,0	4,60	0,9	0,18	0,04	nM
-----	------	------	-----	------	------	----

Peptide-construct

10.000	2.000	400	80	16	3,2	0,64	0,128	0,0256	nM
--------	-------	-----	----	----	-----	------	-------	--------	----

Figure 3.1: Scheme of the different concentrations of AMD3100, AMD11070 and all peptide-constructs that were used in the affinity study.

3.7. CALCIUM-BINDING ASSAY

The lab of Dr. Dominique Schols at the Rega institute (lab of virology and chemotherapy) also kindly performed the calcium-binding assay according to a previously published assay by Claes *et al.* (2018)(66).

For the calcium-binding assay (Figure 3.2), which was also performed twice, the Jurkat cells were seeded in a 96-well plate (black-walled with clear bottom) with an obtained cell density of $0.2 \cdot 10^5$ (viable) cells per well and incubated overnight at 37°C and 5% CO_2 . Next, the cells were loaded with a fluorescent Ca^{2+} -sensitive dye fluo-2 AM. This was done by preparing an assay buffer consisting of 40 mL HEPES (1 M) to 200 mL Hank's Balanced Salt Solution (HBSS) and adding ultrapure water until a final volume of 2 L is obtained. Next, 4 g of Bovine Serum Albumin (BSA) was added and dissolved in the solution. The pH was adjusted to 7.4 by adding sodium hydroxide. After, a stock solution of the fluorescent Ca^{2+} -sensitive dye fluo-2 AM of 4 mM in dimethyl sulfoxide (DMSO) was prepared. Precautions were taken to limit light-exposure of the dye. The stock solution with non-ionic

surfactant polyol solution (20% w/v in DMSO) was diluted to 4 μM of fluorescent Ca^{2+} -sensitive dye fluo-2 AM. The growth medium of the Jurkat cells was removed and 100 μL of loading dye solution was added per well and incubated for 45 min at room temperature in a dark space. A different 96-well plate, made of polypropylene, was prepared containing the CXCL12 solution and the compounds that needed to be tested (DV1-K-(DV3), NOTA-DV1-K-(DV3), AIF-NOTA-DV1-K-(DV3), DOTA-DV1-K-(DV3), Ga-DOTA-DV1-K-(DV3), Lu-DOTA-DV1-K-(DV3) and La-DOTA-DV1-K-(DV3)). Out of a CXCL12 stock solution with a concentration of 1 mg/mL in ultrapure water (0.01% Tween20), a solution of CXCL12 in assay buffer with a concentration of 250 ng/mL (31.25 nM) was made. A solution was made for each construct with a concentration of 250 ng/mL in assay buffer. In one 96-well plate without cells, the CXCL12 solution was added (75 μL /well), in another 96-well plate without cells, the compound solution was added (50 μL /well).

Fluorescence was measured (kinetically) for ± 10 min at defined timepoints. The excitation wavelength was 470-495 nm, the emission wavelength was 515-575 nm. The loading buffer was removed from the 96-well plate containing the Jurkat cells and then the seeded cells were washed and incubated with assay buffer for 2 min with 150 μL /well. The assay buffer was removed again and 80 μL /well of assay buffer was added once more. The plates were put in the device (37°C) and incubated for 5 min. Next, 20 μL of the compound solution (DV1-K-(DV3), NOTA-DV1-K-(DV3), DOTA-DV1-K-(DV3), Ga-DOTA-DV1-K-(DV3), or Lu-DOTA-DV1-K-(DV3)) was added to each well that contained the fluo-2 AM loaded Jurkat cells. The cells were incubated for 10 min and the fluorescence was continuously measured during this period. After, a fixed concentration of CXCL12 was added to each of the wells and fluorescence was also measured.

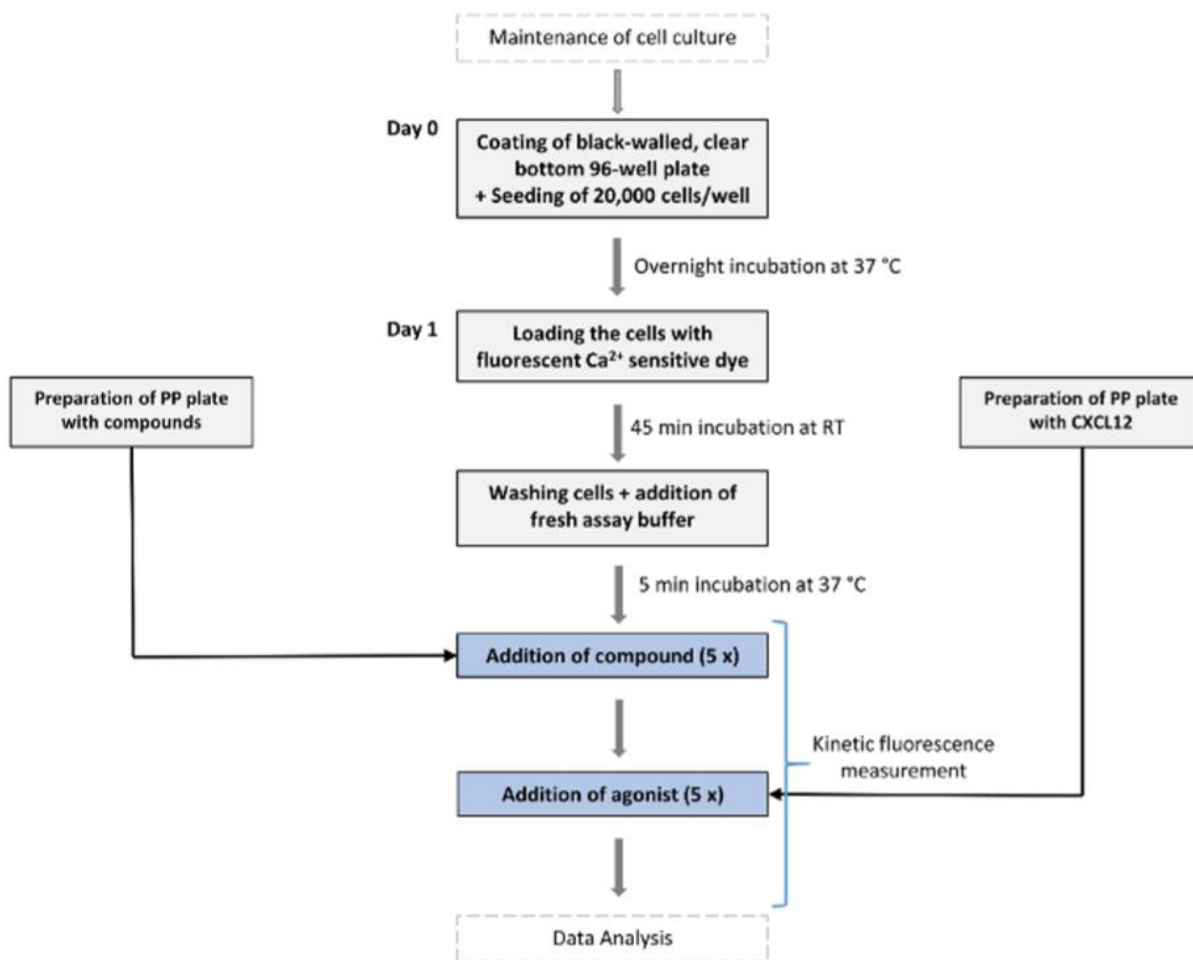


Figure 3.2: Schematic depiction of the workflow used for the calcium mobility assay. On day zero, Jurkat cells expressing the CXCR4 receptor were seeded in 96-well plates (black-walled with clear bottom). These cells were grown overnight at 37°C and 5% CO₂. On day one, the fluorescence-based calcium assay was performed. First, the Jurkat cells were loaded with the fluorescent Ca²⁺-sensitive dye fluo-2 AM and incubated for 45 min at room temperature in a dark environment. A 96-well plate was prepared for the CXCL12 solution and another 96-well plate was prepared using the solutions of the constructs that were tested (DV1-K-(DV3), NOTA-DV1-K-(DV3), DOTA-DV1-K-(DV3), Ga-DOTA-DV1-K-(DV3), or Lu-DOTA-DV1-K-(DV3)). After the incubation with fluo-2 AM, the seeded Jurkat cells were washed once with assay buffer (150 µL/well) and 80 µL/well of assay buffer was added. The plates were put into the device and incubated at 37°C for 5 min. Then, fluorescence was continuously measured while the constructs were added to the wells of the measurement plate and allowed to incubate for ±10 min. Next, a fixed concentration of CXCL12 (the endogenous agonist of the CXCR4 receptor) was added to trigger calcium release. During the addition of the CXCL12 solution and thereafter, the fluorescence was also recorded. PP stands for polypropylene. Figure from Claes et al. (2018)(66).

3.8. QUALITY CONTROL SYSTEM

A Waters XBridge C₁₈ column (3x100 mm, 3.5 µm) with a gradient of ammonium acetate 0.05 M pH 5.5 and ACN at a flowrate of 0.8 mL/min was used as a quality control (QC) system. A detection wavelength of 220 nm was used for all but one run, as the peptide has a maximum absorbance at this wavelength. During Test 9, a wavelength of 280 nm was used. The injected reference solution contained

1 mg/mL DV1-K-(DV3) in H₂O/ACN 50/50% v/v. Table 3.2a and Table 3.2b depict the HPLC gradient compositions that were tested, as well as the wavelength that was used.

Table 3.2a: Scheme of the HPLC gradients that were used to test the quality control system for the peptide-constructs. Ammonium acetate (0.05 M, pH 5.5) is used as the mobile phase with acetonitrile as organic modifier. The column is first rinsed and then equilibrated after each run (30.1-36 min and 35.1-50 min respectively.)

	Ammonium acetate 0.05M pH5.5/ACN				
	Test 1	Test 2	Test 3	Test 4	Test 5
Wavelength	220 nm	220 nm	220 nm	220 nm	220 nm
0 min	95/5	75/25	85/15	90/10	85/15
30 min	5/95	55/45	65/35	75/25	70/30
30.1-35 min	20/80	20/80	20/80	5/95	5/95
35.1-50 min	95/5	75/25	85/15	90/10	85/15

Table 3.2b: Scheme of the HPLC gradients that were used to test the quality control system for the peptide-constructs. Ammonium acetate (0.05 M, pH 5.5) is used as the mobile phase with acetonitrile as organic modifier. The column is first rinsed and then equilibrated after each run (30.1-36 min and 35.1-50 min respectively for Test 6 and 7 and 22-25 min and 27-35 min respectively for Test 8 and 9.)

	Ammonium acetate 0.05M pH5.5/ACN				
	Test 6	Test 7		Test 8	Test 9
Wavelength	220 nm	220 nm	Wavelength	220 nm	280 nm
0 min	85/15	85/15	0 min	90/10	90/10
30 min	75/25	80/20	20 min	70/30	70/30
30.1-35 min	5/95	5/95	22-25 min	5/95	5/95
35.1-50 min	85/15	85/15	27-35 min	90/10	90/10

3.9. RADIOSYNTHESIS OF [¹⁸F]AlF-NOTA-DV1-K-(DV3)

Protons accelerated in the cyclotron were used to irradiate [¹⁸O]H₂O to produce the [¹⁸F]F⁻. In the Trasis AllinOne module, the produced [¹⁸F]F⁻ was trapped onto an QMA anion exchange cartridge and subsequently eluted with NaCl 0.9%/absolute ethanol (QMA eluent) to produce [¹⁸F]NaF. To this [¹⁸F]NaF solution, AlCl₃ (25 μL, 2 mM in sodium acetate buffer 0.1 M, pH 4.1) was added and this solution was incubated at room temperature for 2 min to produce [¹⁸F]AlF. The NOTA-DV1-K-(DV3) (100 nmol, sodium acetate buffer 0.1 M pH 4.1; absolute EtOH (50/50% v/v) was added to the reactor containing [¹⁸F]AlF and the reactor was heated to 100°C for 10 min (Figure 3.3). The resulting [¹⁸F]AlF-NOTA-DV1-K-(DV3) was purified using a preconditioned SPE Sep-Pak C₁₈ cartridge and formulated

using absolute ethanol (8%), sodium ascorbate (0.59%), and NaCl (0.9%). As a final step, sterile filtration was performed using a Millex-GV 13 mm (0.22 µm) filter and the solution was collected in a sterile vial. The [¹⁸F]AlF-NOTA-DV1-K-(DV3) was analysed using a radio-LC-MS system (Short_gradient, HCOOH) and with instant thin layer chromatography (0.9% NaCl as eluent).

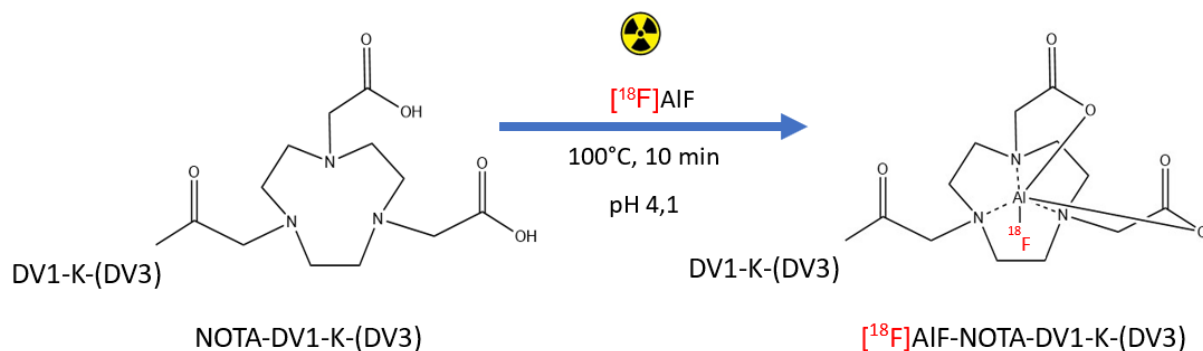


Figure 3.3: Radiolabelling of DV1-K-(DV3)-bound NOTA chelator with [¹⁸F]AlF.

3.10. PHARMACOKINETICS OF [¹⁸F]AlF-NOTA-DV1-K-(DV3)

3.10.1. µPET/CT

The animal ethical committee approval number for the project is LA1210261. Nine mice were used for this study, five received only [¹⁸F]AlF-NOTA-DV1-K-(DV3), two received [¹⁸F]AlF-NOTA-DV1-K-(DV3) and 2.5 mg AMD3100/kg body weight and the last two received [¹⁸F]AlF-NOTA-DV1-K-(DV3) and 5 mg AMD3100/kg body weight. Each mouse received 120 µL (30 MBq/mL) of [¹⁸F]AlF-NOTA-DV1-K-(DV3), administered intravenously. As some of the mice also received a blocking agent, co-injection of the tracer and the blocking agent was performed. As a previous experiment indicated a 50% loss due to activity retention on the catheter, a correction was applied to ensure the mice were given a high enough dose of blocking agent. A dynamic µPET scan, coupled with a CT scan, was taken during a period of 60 min. The mice were injected and scanned while under anaesthesia (2.5% isoflurane in O₂ at a flow rate of 1 L/min). The activity in the organs is expressed as the standardized uptake value (SUV, unitless).

$$\text{SUV} = \frac{\left(\frac{\text{activity in organ}}{\text{organ volume}} \right)}{\left(\frac{\text{injected activity}}{\text{total body mass of animal}} \right)}$$

$$= \frac{\text{organ concentration}}{\text{average concentration}}$$

3.10.2. Biodistribution study

A biodistribution study was performed on the mice after completion of the μ PET scan (both with and without blocking agent). The animals were sacrificed 75 min p.i. while still under anaesthesia, dissected and the organs were counted in the automated 1480 Wizard 3q gamma counter. The activity in the tail of the mice was not taken into account for calculation of the total counts injected. The counts per minute for all the organs were corrected for decay and counter deadtime. Total body weight and organ weight were taken into account to calculate the SUV. The activity in the organs is expressed as the SUV.

$$\begin{aligned} \text{SUV} &= \frac{\left(\frac{\text{activity in organ}}{\text{organ mass}}\right)}{\left(\frac{\text{injected activity}}{\text{total body mass of animal}}\right)} \\ &= \frac{\text{local radioactivity concentration}}{\left(\frac{\text{injected activity}}{\text{body weight}}\right)} \quad (67) \\ &= \frac{\text{organ concentration}}{\text{average concentration}} \end{aligned}$$

4. RESULTS

4.1. SYNTHESIS AND PURIFICATION OF RESCA-DV1-K-(DV3)

RESCA-DV1-K-(DV3) was synthesized and subsequently purified using preparative HPLC. LC-MS data was collected to ascertain the chemical purity of the construct after purification. 254 nm was chosen as the optimal wavelength for the UV-signal for RESCA-DV1-K-(DV3) after making a Diode-Array Detection spectrum of RESCA-DV1-K-(DV3). The Compass Isotope average neutral mass of the RESCA-DV1-K-(DV3) compounds ($C_{187}H_{284}N_{54}O_{48}S_2$) is 4120.71 g/mol. The HPLC UV-chromatogram (254 nm) shows the chemical purity of the collected RESCA-DV1-K-(DV3) (Figure 4.1).

The Average Mass of the construct was 4120.66 g/mol with a Standard Deviation (SD) of 0.02 g/mol (Figure 4.2). The purification of RESCA-DV1-K-(DV3) was successful, with a high chemical purity. HPLC purification using a C_{18} prep column was used, and the RESCA-DV1-K-(DV3) construct had a retention time (Rt) of ± 12 min 30 s. This peak was collected and subsequently dried under vacuum. The purified compound was then dissolved in 1 mL metal-free water and 440 μ L ACN (LC-MS grade) and lyophilised. After, the vial was filled with N_2 gas, covered in aluminium foil and stored in the freezer (-20°C). The total amount of RESCA-DV1-K-(DV3) that was obtained after purification was 6.32 mg (7.67% yield), with a chemical purity $> 95\%$ (Figure 4.1).

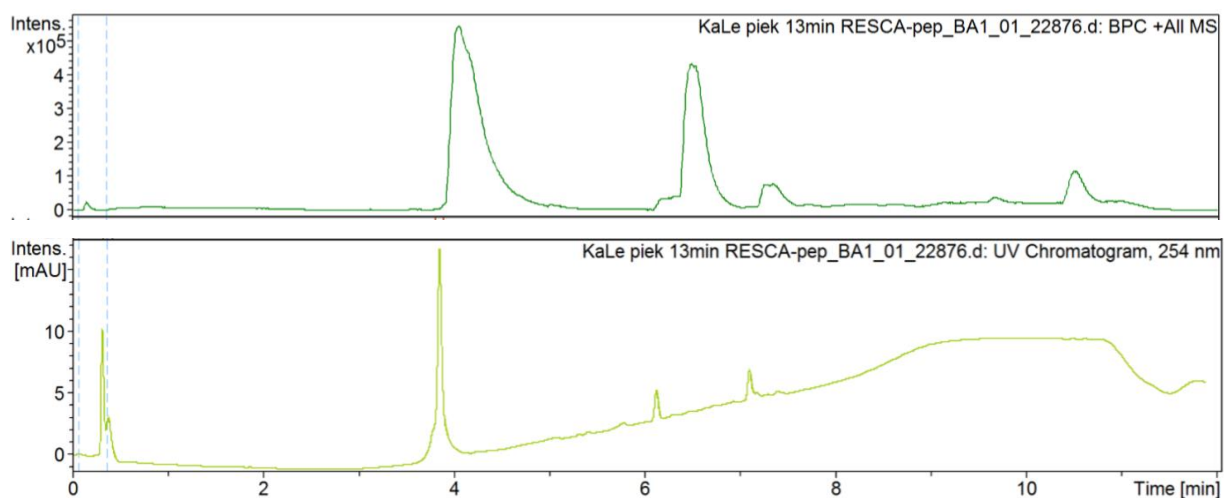


Figure 4.1: Base peak chromatogram of all molecular masses after LC-MS (top chromatogram). HPLC analysis (254 nm) of the RESCA construct after purification. RESCA-DV1-K-(DV3) elutes at about 4 min (lower chromatogram). The peaks at 6 and 7 min were also present in the blank run. (Tune positive mid-range applied voltage LC-MS with a short gradient (HCOOH) was used.)

+MS, 4.0-4.2min #480-503

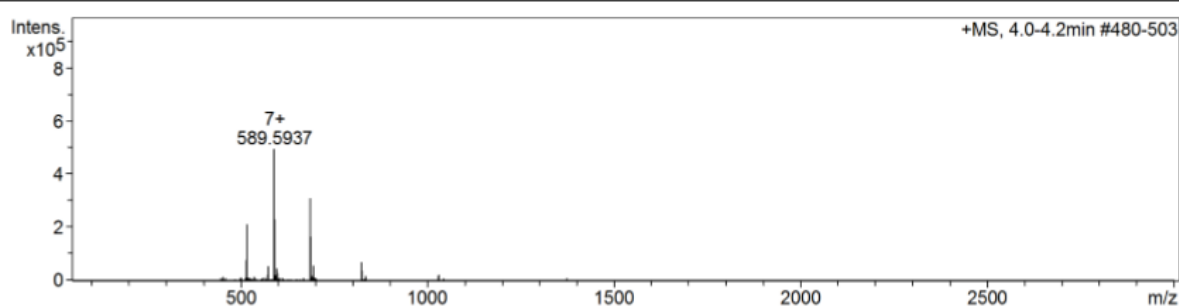


Figure 4.2: MS results of the purification of RESCA-DV1-K-(DV3) of the peak at 4.0-4.2 min. (Tune positive mid-range applied voltage LC-MS with a short gradient (HCOOH) was used.)

4.2. FITC-DV1-K-(DV3) SYNTHESIS

A FITC-construct was made to be able to perform tests to examine the subcellular CXCR4 distribution in tumour tissue. For FITC itself, there were three absorption maxima (Figure 4.3). The first maximum would not allow specific detection of the compound, as many compounds absorb at low wavelengths. The two other maxima were at 280 nm and at 450 nm. At 450 nm, only a broad, low intensity peak was observed. However, after HPLC analysis of the FITC-DV1-K-(DV3) construct after microcleavage, there was no defined peak at 450 nm (Figure 4.4). Therefore 280 nm seems to be the best wavelength for the detection of FITC-DV1-K-(DV3).

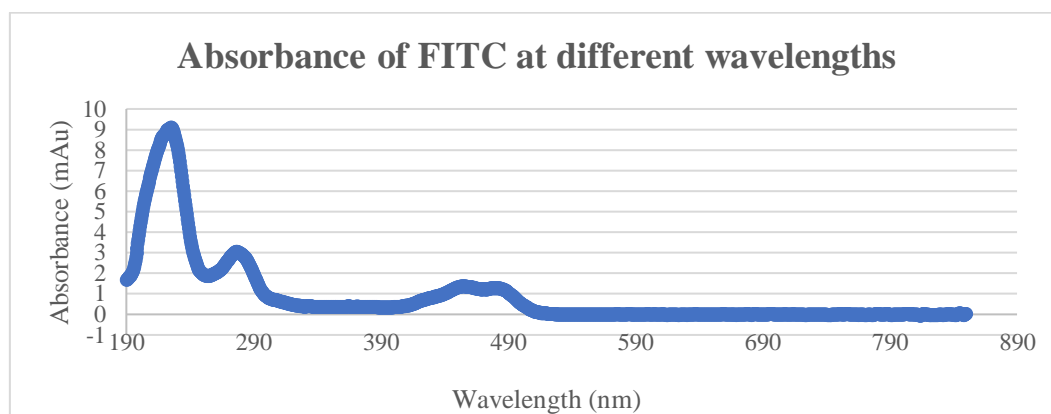


Figure 4.3: UV spectrum of FITC. The absorbance of FITC was determined at different wavelengths on a Fisher Scientific Nanodrop 2000 .

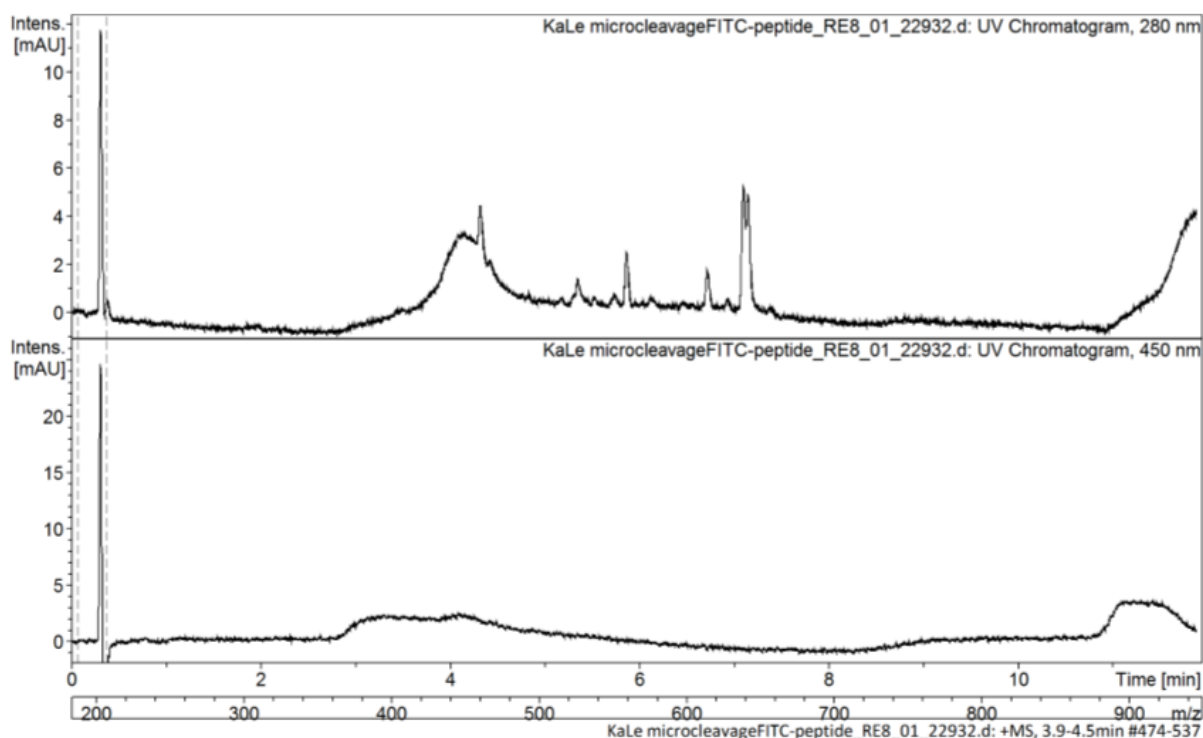


Figure 4.4: HPLC analysis at 280 nm (upper chromatogram) and at 450 nm (lower chromatogram) of the FITC construct after microcleavage. FITC-DV1-K-(DV3) elutes at about 4 min. (Tune positive mid-range applied voltage LC-MS with a short gradient (HCOOH) was used.)

The Compass Isotope average neutral mass of FITC-DV1-K-(DV3) ($C_{187}H_{269}N_{53}O_{46}S_3$) is 4091.67 g/mol. The Average Mass of the construct after microcleavage was 4098.83 g/mol with a SD of 0.07 g/mol (Figure 4.5), indicating that the desired compound was synthesized. However, looking at Figure 4.4, it appears to contain contaminations. For the FITC-DV1-K-(DV3) construct, only a microcleavage was performed, the actual cleavage and purification of the construct using the HPLC system still needs to be performed.

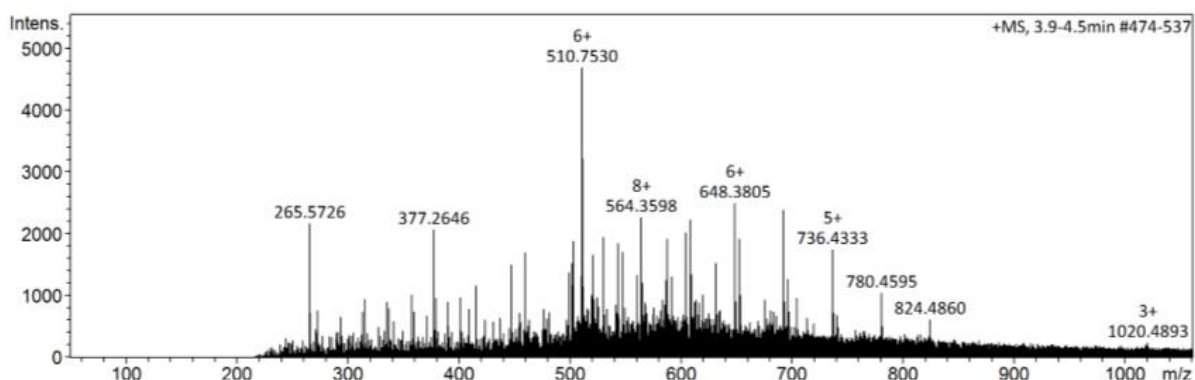


Figure 4.5: MS results of the microcleavage of FITC-DV1-K-(DV3). (Tune positive mid-range applied voltage LC-MS with a short gradient (HCOOH) was used.)

4.3. LABELLING WITH STABLE ISOTOPES

220 nm was chosen as the optimal wavelength for the UV-signal for all constructs, as the DV1-K-(DV3) peptide has an absorbance maximum at this wavelength. The Compass Isotope average neutral mass of NOTA-DV1-K-(DV3) ($C_{178}H_{277}N_{55}O_{46}S_2$) is 3987.58 g/mol and is 4088.69 g/mol for DOTA-DV1-K-(DV3) ($C_{182}H_{284}N_{56}O_{48}S_2$).

4.3.1. $^{nat}F^-$ -AIF-labelling of NODA-MP-NCS

The labelling of NODA-MP-NCS with AIF was performed as a test to see whether or not the protocol that was described, is appropriate to use for the $^{nat}F^-$ -AIF-labelling of NOTA-DV1-K-(DV3). The test labelling used the NODA-MP-NCS-chelator without the peptide attached to it. The Compass Isotope average neutral mass of AIF(NODA)-MP-NCS ($C_{18}H_{22}N_4O_4SAIF$) is 436.44 g/mol (Figure 4.6). At first sight, the complexation of stable AIF did not seem to work using this protocol, as the desired mass was not observed. More tests need to be performed to optimize the method before it can be used to synthesise AIF-NOTA-DV1-K-(DV3).

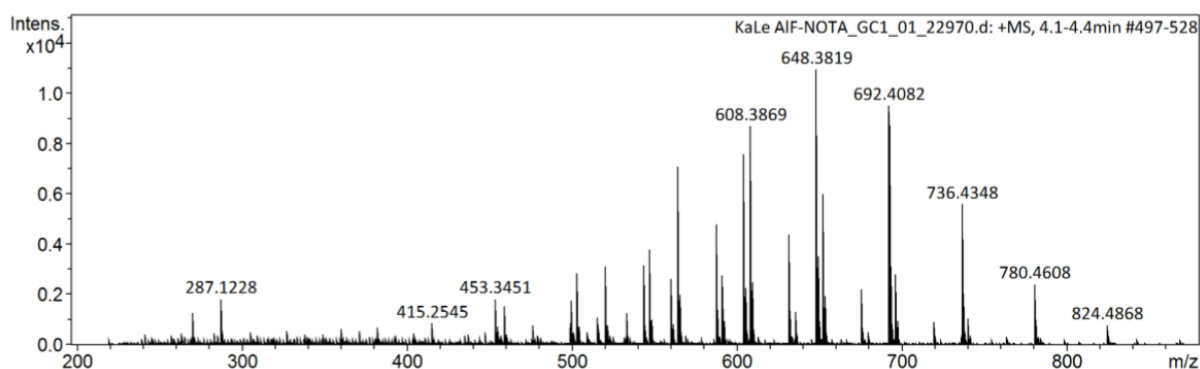


Figure 4.6: MS results of the cold labelling of NODA-MP-NCS with aluminium fluoride. (Tune positive mid-range applied voltage LC-MS with a short gradient (HCOOH) was used.)

4.3.2. $^{nat}Ga^{3+}$ -labelling of NOTA-DV1-K-(DV3)

Ga-NOTA-DV1-K-(DV3) was synthesized to use in affinity tests and calcium-binding assays, in case the fluorine-18 tracer encountered issues such as if the $[^{18}F]AIF-NOTA/RESCA$ PK profile would not match that of $[^{225}Ac]/[^{177}Lu]-DOTA-DV1-K-(DV3)$. The Compass Isotope average neutral mass of Ga-NOTA-DV1-K-(DV3) ($C_{178}H_{275}N_{55}O_{46}S_2Ga$) is 4055.29 g/mol. The Average Mass of the construct was 4053.12 g/mol with a SD of 0.02 g/mol (Figure 4.7).

HPLC analysis (220 nm) shows the purity of the Ga-NOTA-DV1-K-(DV3) (Figure 4.8). The total amount of Ga-NOTA-DV1-K-(DV3) that was obtained after purification through a Sep-Pak Plus Light C_{18} cartridge was 0.81 mg (98.64% yield), with a chemical purity of 78% (Table 4.1). Sadly, no blank injection test was carried out. The chemical purity is likely higher than the reported percentage, as many

of the small peaks are likely due to artefacts of the system, as the starting material NOTA-DV1-K-(DV3) was pure (> 95%). The purified compound was then dissolved in 1 mL metal-free water and 440 μ L ACN (LC-MS grade) and lyophilised (Figure 4.9). After, the vial was filled with N₂ gas, covered in aluminium foil and stored in the freezer (-20°C).

+MS, 3.8-4.0min #451-475

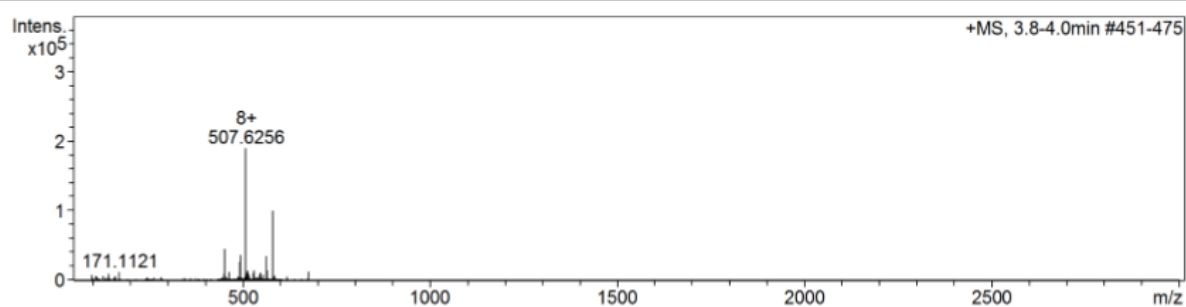


Figure 4.7: MS results of the cold labelling of NOTA-DV1-K-(DV3) with gallium. (Tune positive mid-range applied voltage LC-MS with a short gradient (HCOOH) was used.)

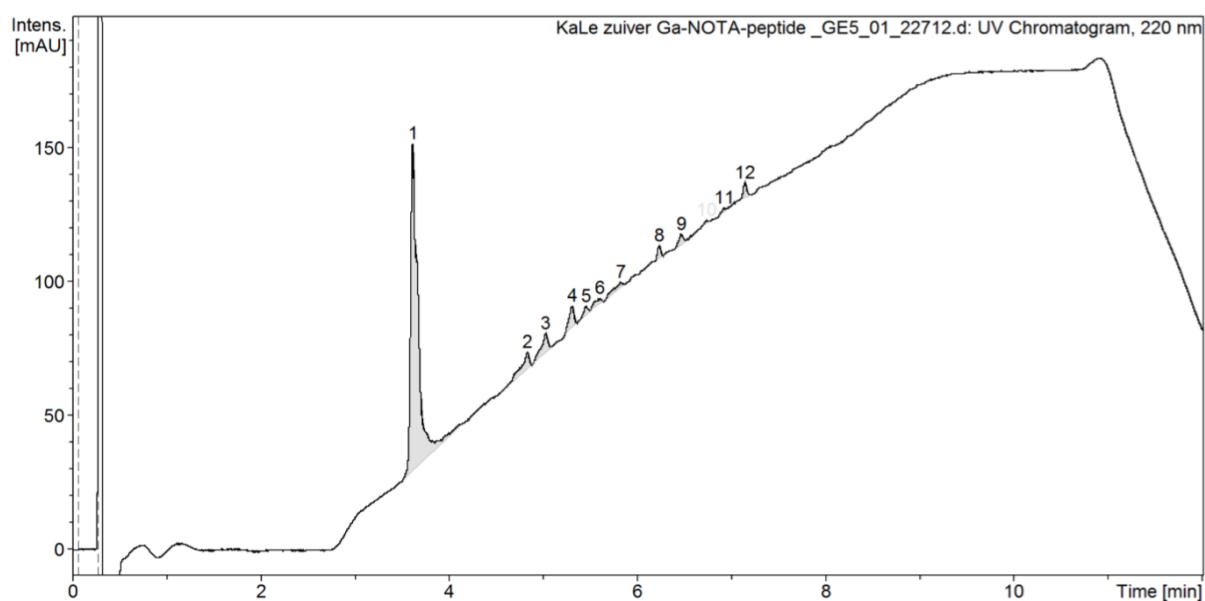


Figure 4.8: HPLC analysis (220 nm) of the cold construct with gallium (Ga-NOTA-DV1-K-(DV3)). (Tune positive mid-range applied voltage LC-MS with a short gradient (HCOOH) was used.)

Table 4.1: MS results of Ga-NOTA-DV1-K-(DV3). Rt stands for retention time; Area Frac. stands for fraction of the area.

# peak	Rt (min)	Area (mV/s)	Area Frac. (%)
1	3.6	656	78
2	4.8	37	4
3	5.0	34	4
4	5.3	27	3
5	5.5	10	1
6	5.6	11	1
7	5.8	17	2
8	6.2	10	1
9	6.5	13	2
10	6.7	2	0.3
11	6.9	4	0.4
12	7.1	13	2



Figure 4.9: Lyophilized cold construct of Ga-NOTA-DV1-K-(DV3).

4.3.3. $^{nat}\text{Ga}^{3+}$ -labelling of DOTA-DV1-K-(DV3)

Ga-DOTA-DV1-K-(DV3) was synthesized to use in affinity tests and calcium-binding assays, in case the F-NOTA-DV1-K-(DV3) compound encountered issues such as if the ^{18}F]AlF-NOTA/RESCA PK profile would not match that of ^{225}Ac]/ ^{177}Lu]-DOTA-DV1-K-(DV3). The Compass Isotope average neutral mass of Ga-DOTA-DV1-K-(DV3) ($\text{C}_{182}\text{H}_{281}\text{N}_{56}\text{O}_{48}\text{S}_2\text{Ga}$) is 4155.38 g/mol. The Average Mass of the construct was 4153.66 g/mol with a SD of 0.01 g/mol (Figure 4.10). HPLC analysis (220 nm) shows the chemical purity of the Ga-DOTA-DV1-K-(DV3) (Figure 4.11). The purified compound was then dissolved in 1 mL metal-free water and 440 μL ACN (LC-MS grade) and lyophilised. After, the vial was filled with N_2 gas, covered in aluminium foil and stored in the freezer (-20°C). The total amount of Ga-DOTA-DV1-K-(DV3) that was obtained after purification through a Sep-Pak Plus Light C_{18} cartridge was 0.62 mg (66.31% yield), with a chemical purity of $> 95\%$ (Figure 4.11).

+MS, 3.6-3.7min #434-440

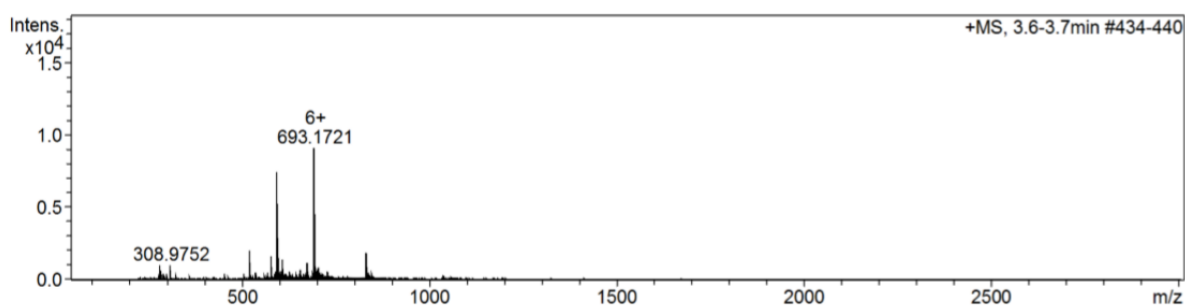


Figure 4.10: MS results of the cold labelling of DOTA-DV1-K-(DV3) with gallium. (Tune positive mid-range applied voltage LC-MS with a short gradient (HCOOH) was used.)

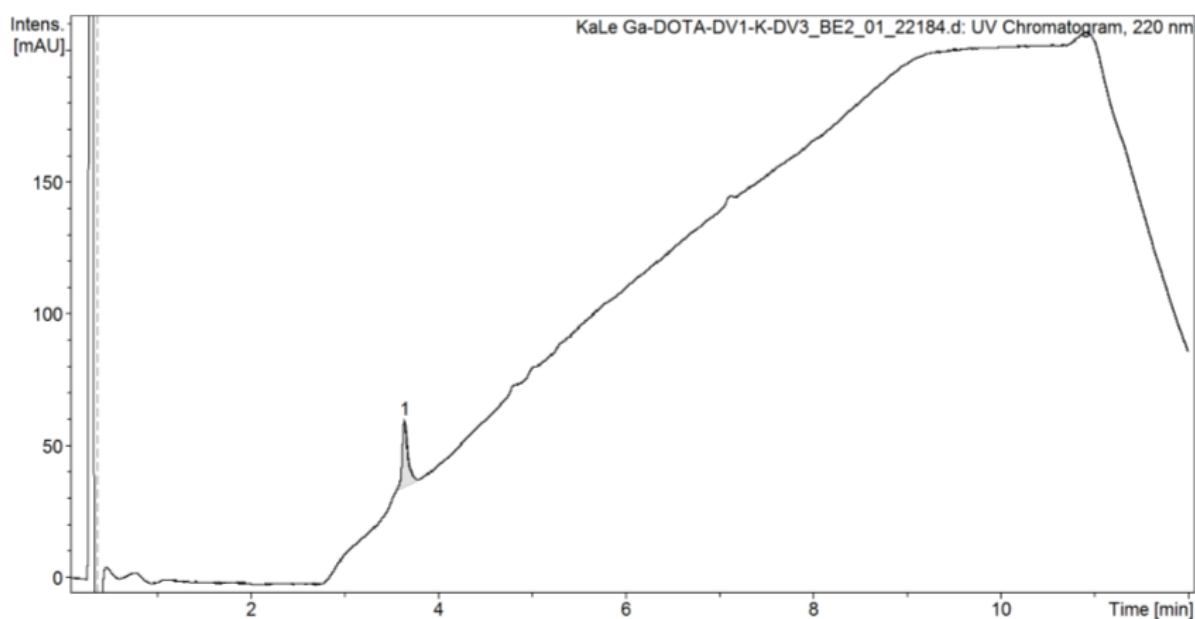


Figure 4.11: HPLC analysis (220 nm) of the cold construct with gallium (Ga-DOTA-DV1-K-(DV3)). (Tune positive mid-range applied voltage LC-MS with a short gradient (HCOOH) was used.)

4.3.4. $^{nat}\text{Lu}^{3+}$ -labelling of DOTA-DV1-K-(DV3)

Lu-DOTA-DV1-K-(DV3) was synthesized to use in affinity tests and calcium-binding assays, to ascertain the potential of [^{177}Lu]Lu-DOTA-DV1-K-(DV3) as an accompanying therapeutic radiopharmaceutical for [^{18}F]AlF-NOTA-DV1-K-(DV3). The Compass Isotope average neutral mass of Lu-DOTA-DV1-K-(DV3) ($\text{C}_{182}\text{H}_{281}\text{N}_{56}\text{O}_{48}\text{S}_2\text{Lu}$) is 4260.63 g/mol. The Average Mass of the construct was 44259.14 g/mol with a SD of 0.01 g/mol (Figure 4.12). HPLC analysis (220 nm) shows the chemical purity of the Lu-DOTA-DV1-K-(DV3) (Figure 4.13). The purified compound was then dissolved in 1 mL metal-free water and 440 μL ACN (LC-MS grade) and lyophilised. After, the vial was filled with N_2 gas, covered in aluminium foil and stored in the freezer (-20°C). The total amount of Lu-DOTA-DV1-K-(DV3) that was obtained after purification through a Sep-Pak Plus Light C_{18} cartridge was 0.81 mg (84.49% yield), with a chemical purity of $> 95\%$ (Figure 4.13).

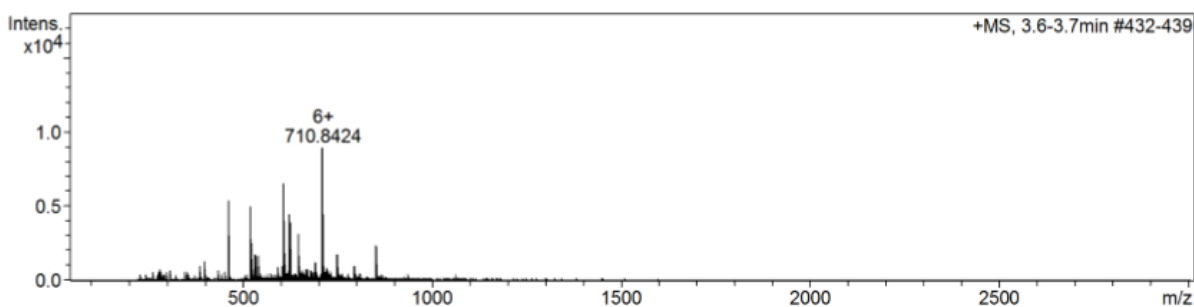


Figure 4.12: MS results of the cold labelling of DOTA-DV1-K-(DV3) with lutetium. (Tune positive mid-range applied voltage LC-MS with a short gradient (HCOOH) was used.)

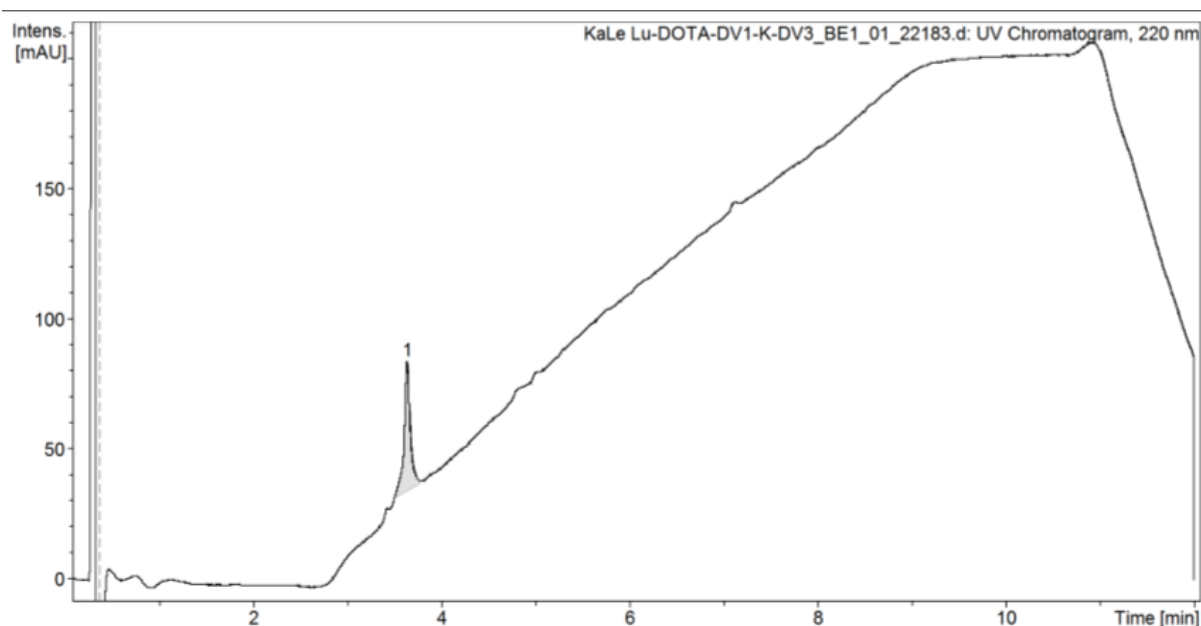


Figure 4.143: HPLC analysis (220 nm) of the cold construct with lutetium (Lu-DOTA-DV1-K-(DV3)). (Tune positive mid-range applied voltage LC-MS with a short gradient (HCOOH) was used.)

4.3.5. $^{nat}\text{La}^{3+}$ -labelling of DOTA-DV1-K-(DV3)

La-DOTA-DV1-K-(DV3) was synthesized to use in affinity tests and calcium-binding assays, to ascertain the potential of $[^{225}\text{Ac}]\text{Ac-DOTA-DV1-K-(DV3)}$ as an accompanying therapeutic radiopharmaceutical for $[^{18}\text{F}]\text{AlF-NOTA-DV1-K-(DV3)}$. The Compass Isotope average neutral mass of La-DOTA-DV1-K-(DV3) ($\text{C}_{182}\text{H}_{281}\text{N}_{56}\text{O}_{48}\text{S}_2\text{La}$) is 4224.57 g/mol. The Average Mass of the construct was 4222.73 g/mol with a SD of 0.02 g/mol (Figure 4.14). LC-MS is a very precise method of detection and therefore La-DOTA-DV1-K-(DV3) was detectable, with a slight deviation in regards to the Compass Isotope average neutral mass. However, the peak of the construct was not visible in any of the HPLC UV chromatograms, indicating a very low yield and therefore indicating that the protocol that was described was not appropriate for the labelling of DOTA-DV1-K-(DV3) with ^{nat}La .

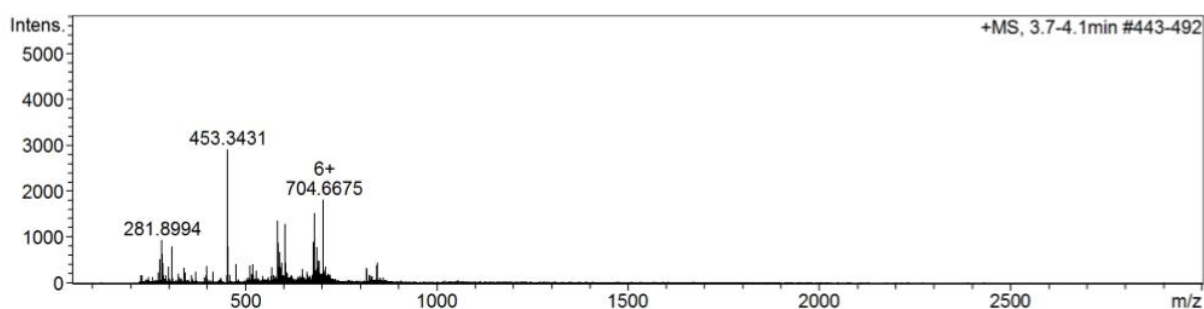


Figure 4.1 4: MS results of the cold labelling of DOTA-DV1-K-(DV3) with lanthanum. (Tune positive mid-range applied voltage LC-MS with a short gradient (HCOOH) was used.)

4.4. AFFINITY TESTS

Affinity tests were performed to ascertain whether or not the constructs retained their affinity after modification of the vector molecule. The affinity test was performed twice. Figure 4.15 depicts the graphs of concentration of the compound (nM) in terms of % inhibition of CXCL12-AF647 binding in Jurkat cells. The data used in the graph is the average of the two affinity assays that were performed. A few of the constructs were not tested, as the lockdown interfered with the schedule: Ga-NOTA-DV1-K-(DV3), RESCA-DV1-K-(DV3), AIF-RESCA-DV1-K-(DV3), La-DOTA-DV1-K-(DV3) and FITC-DV1-K-(DV3). The affinity tests yielded IC_{50} 's for the tested compounds (Table 4.2).

Table 4.2: IC_{50} 's of the two affinity tests of the tested compounds (AMD3100, AMD11070, DV1-K-(DV3), NOTA-DV1-K-(DV3), DOTA-DV1-K-(DV3), Ga-DOTA-DV1-K-(DV3) and Lu-DOTA-DV1-K-(DV3).

Compound	Average IC_{50} (nM)
AMD3100	11.47
AMD11070	4.24
DV1-K-(DV3)	16.47
DOTA-DV1-K-(DV3)	228.4
Ga-DOTA-DV1-K-(DV3)	12.09
Lu-DOTA-DV1-K-(DV3)	5.43
NOTA-DV1-K-(DV3)	107.7

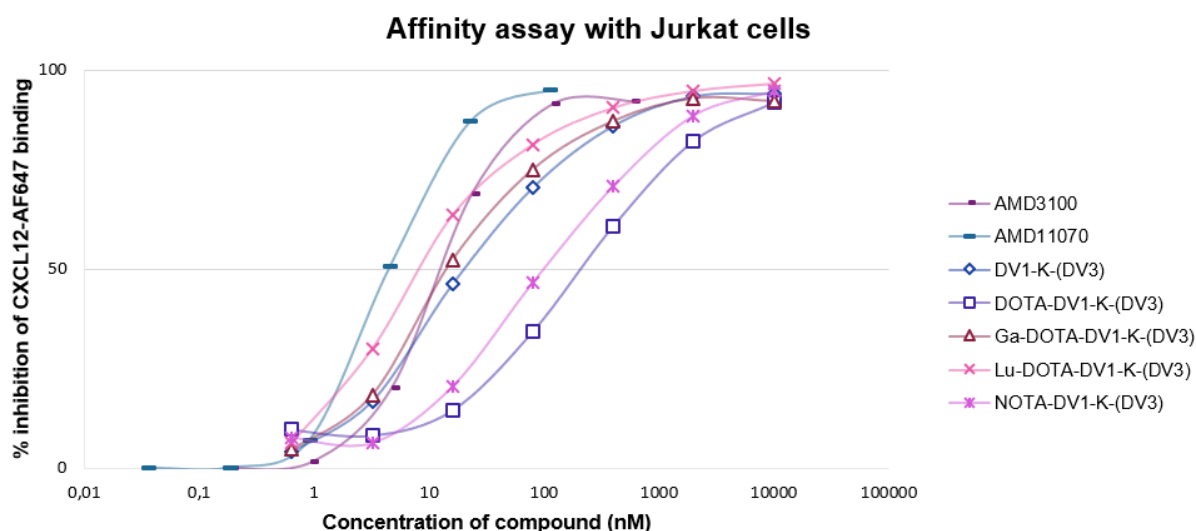


Figure 4.15: Affinity test of several peptide constructs and two known CXCR4 receptor inhibitors (AMD3100 and AMD11070) and their inhibition of the CXCL12 binding to the CXCR4 receptor. Data is depicted as % inhibition of binding of the fluorescently-labelled CXCL12 to Jurkat cells in relation to the concentration of the inhibitor (AMD3100, AMD11070 or a peptide-construct). The data used is the average of the two affinity assays that were performed.

4.5. CALCIUM-BINDING ASSAY

A calcium-binding assay was performed to ascertain whether the constructs retained their activity (their ability to inhibit the function of CXCR4) after modification of the vector molecule. The calcium-binding assay data was performed twice. Figure 4.16 depicts the graphs of concentration of the compound (nM) in terms of % inhibition of CXCL12-induced calcium response in Jurkat cells. The data used in the graph is the average of the two inhibitory activity tests that were performed. A few of the constructs were not tested, as the lockdown interfered with the schedule: Ga-NOTA-DV1-K-(DV3), RESCA-DV1-K-(DV3), AIF-RESCA-DV1-K-(DV3), La-DOTA-DV1-K-(DV3) and FITC-DV1-K-(DV3).

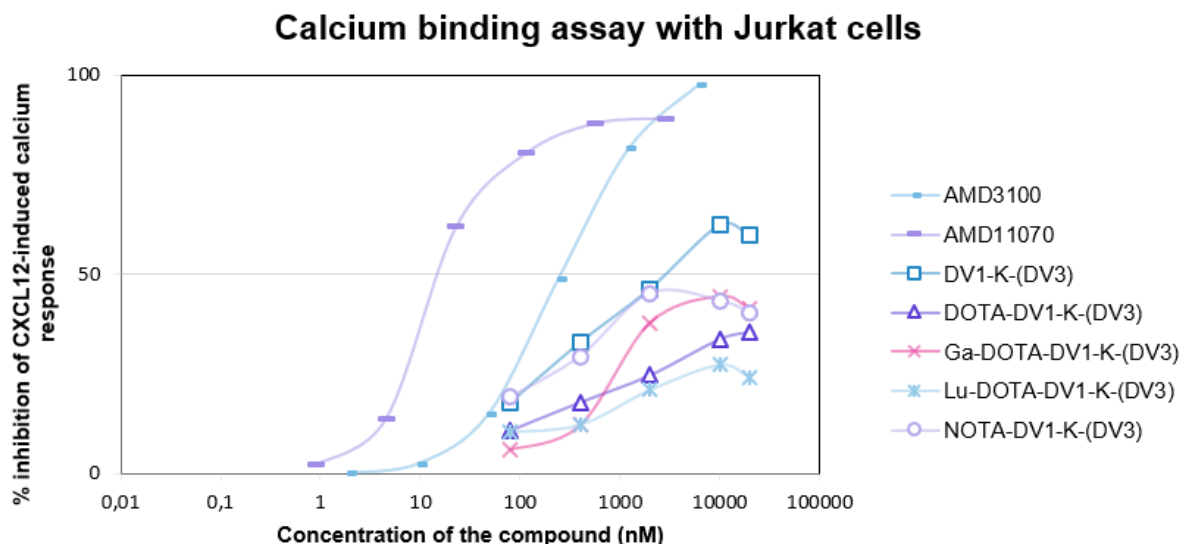


Figure 4.16: Calcium mobilisation test of different peptide-constructs and two known CXCR4 receptor inhibitors (AMD3100 and AMD11070). The IC₅₀ of AMD3100 is about 263.5 nM and the IC₅₀ of AMD11070 is about 13.26 nM. The data used is the average of the two calcium-binding assays that were performed.

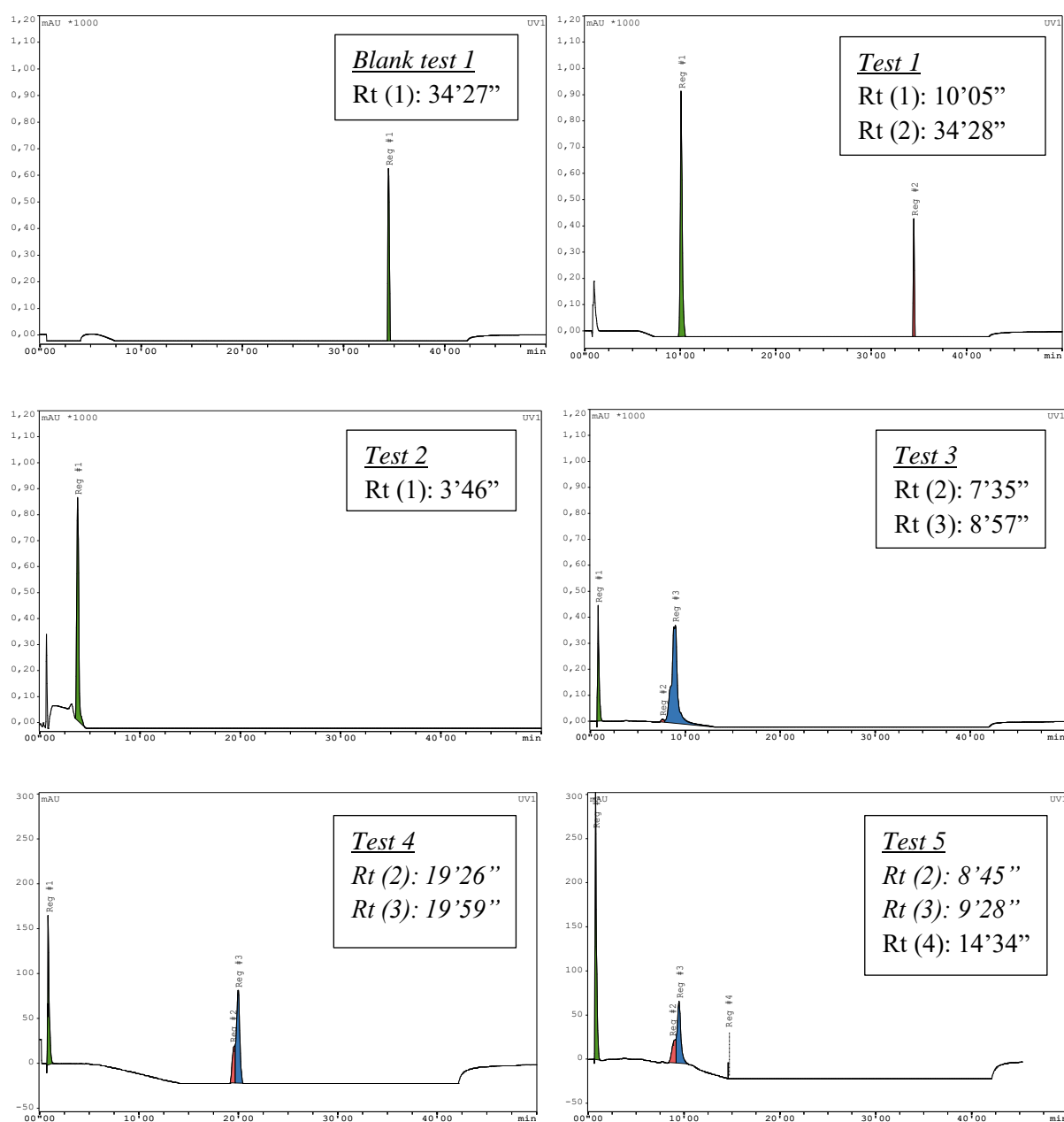
4.6. QUALITY CONTROL SYSTEM

Obtaining a good QC system is vital for translation of radiopharmaceutical research to a clinical setting. A Rt of about 12 min was determined to be favourable for the QC system. As there are only minor structural differences between DV1-K-(DV3) and the different DV1-K-(DV3)-based radiopharmaceuticals, the same QC system can probably be used for all these DV1-K-(DV3)-based constructs.

Figure 4.17 depicts different HPLC chromatograms of HPLC conditions that were tested using the reference solution (DV1-K-(DV3) 1 mg/mL in H₂O/ACN 50/50 v/v%). The conditions were adapted until the peak shape was symmetrical and the Rt was about 12 min.

In Test 1, the Rt was about 34 min 30 s, which was too long. Therefore, the gradient was adapted to contain more ACN at the beginning of the run and to have a less steep gradient. In Test 1, the second peak is a peak that was also present in the blank (blank Test 1). The reference had a Rt of about 4 min at the conditions of Test 2, which was too soon. In Test 3, the gradient was adapted again to contain a lower percentage of ACN at the start of the run and an even less steep gradient was used. The adaptations to the mobile phase resulted in a Rt of about 19 min 30 s for Test 3. Next, in Test 4 the gradient system was adapted to contain an even lower percentage of ACN at the start of the run and the gradient was less steep than in Test 3. In Test 5, the gradient system was adapted to start with the same v/v% H₂O/ACN as in Test 3, as this was considered more favourable in terms of Rt than Test 4. In Test 6, the starting v/v% H₂O/ACN was identical to Test 5, but the gradient was less steep. In Test 7, the starting point was

again kept identical to Test 5 and Test 6, but the steepness of the gradient was decreased again. The Rt of Test 7 was the most preferable. However, peak splitting was observed and needed further examination, as only one molecule was supposed to be eluting (DV1-K-(DV3)). A possible explanation can be degradation of the stock solution. The peaks are separated better in Test 7 than they are in Test 6. In Tests 8 and 9, the gradient system was adapted again to the system that is currently used. With this QC system, a single peak was obtained with $Rt \pm 13 \text{ min } 30 \text{ s}$ using a freshly prepared aliquot of DV1-K-(DV3) 1 mg/mL in H₂O/ACN 50/50 v/v% (Figure 4.17; Test 8). 280 nm was also tried as wavelength, to see whether or not the baseline was more stable than at 220 nm and whether DV1-K-(DV3) was still detectable at this wavelength (Test 9). A wavelength of 280 nm is suitable for the detection of DV1-K-(DV3) and has a stable baseline for the gradient system.



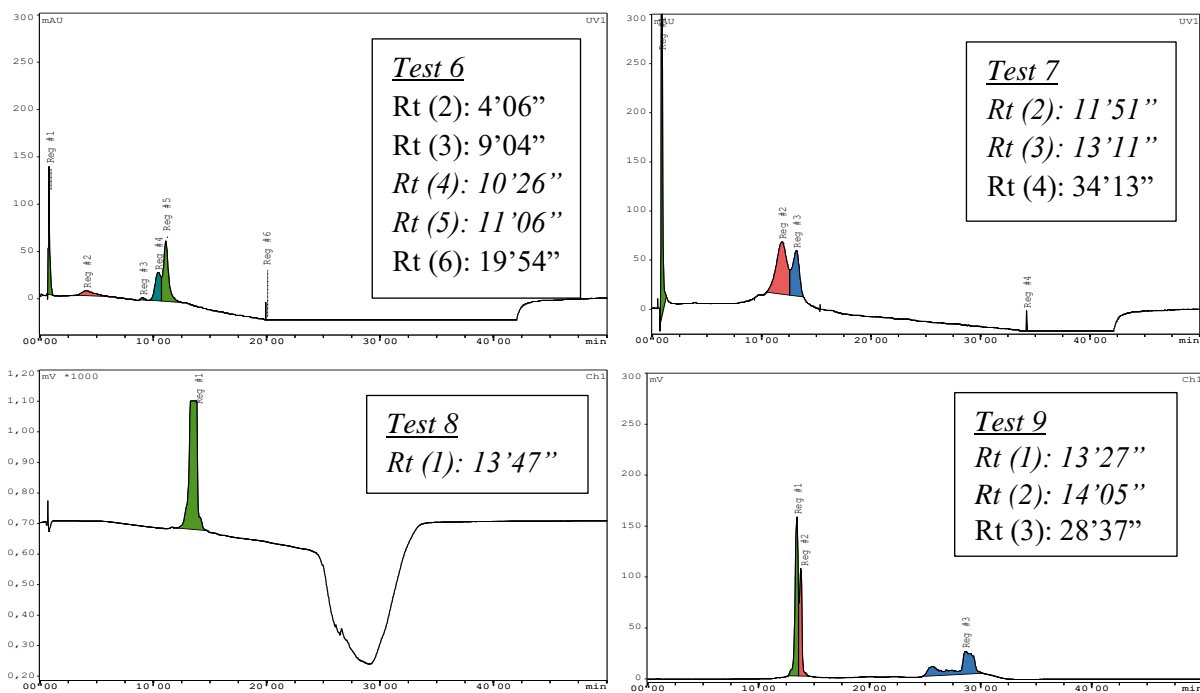


Figure 4.17: HPLC chromatograms of the QC system of DV1-K-(DV3). Several gradient systems were tested and each time the reference consisted of DV1-K-(DV3) 1 mg/mL in H₂O/ACN 50/50 v/v%. Tests 1-8 were performed at 220 nm, Test 9 was performed at 280 nm. Tests 1 through 7 were performed using one stock solution during several days. Tests 8 and 9 were performed using a new stock solution. (Waters XBridge C₁₈, 3x100 mm, 3.5 μm; ammonium acetate 0.05 M pH 5.5/ACN; 0.8 mL/min).

In tests 10 and 11 (Figure 4.18), the HPLC runs were performed using an isocratic system with a mobile phase composition of ammonium acetate 0.05 M pH 5.5/ACN 85/15 v/v%. An isocratic system was tested to see whether it would improve the separation of the peaks that seemed to be co-eluting at the Rt of the reference. Test 10 was performed using an ‘old’ aliquot, to test the amount of degradation product. Test 11 was performed using a fresh aliquot, to be able to compare an old and a fresh aliquot and determine the difference in composition and in chromatograms. As only one major peak eluted when using a fresh aliquot, degradation of the stock solution needs to be considered.

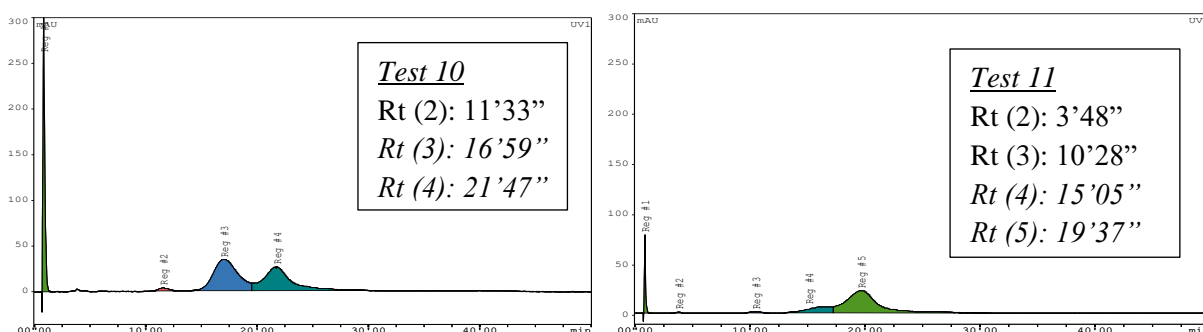


Figure 4.18: HPLC chromatograms of the QC system of DV1-K-(DV3) with DV1-K-(DV3) 1 mg/mL in H₂O/ACN 50/50 v/v% as the reference that was used. Test 10 was performed using an old aliquot, Test 11 was performed with a fresh aliquot. The retention time of the solvent peak is not given. (Waters XBridge C₁₈, 3x100 mm, 3.5 μm; ammonium acetate 0.05 M pH 5.5/ACN 85/15 v/v%; 0.8 mL/min; 220 nm).

4.7. PHARMACOKINETICS OF [¹⁸F]AIF-NOTA-DV1-K-(DV3)

4.7.1. μ PET/CT

The purified [¹⁸F]AIF-NOTA-DV1-K-(DV3) had a yield of 1.07 GBq, and a radiochemical purity of > 95%. μ PET/CT scans were performed in healthy mice to determine the PK properties of [¹⁸F]AIF-NOTA-DV1-K-(DV3), both with and without the blocking agent AMD3100 (CXCR4 antagonist). The [¹⁸F]AIF-NOTA-DV1-K-(DV3) μ PET/CT scans of the naïve mice showed fast clearance and high activity in the kidneys, bladder, and liver. Some activity was also visible in the joints. When both [¹⁸F]AIF-NOTA-DV1-K-(DV3) and AMD3100 were injected, the uptake in the liver decreased and the uptake in the kidneys increased. The activity was also blocked in the joints after administration of AMD3100, indicating specific binding of [¹⁸F]AIF-NOTA-DV1-K-(DV3) in the bone marrow (Figures 4.19 and 4.20).

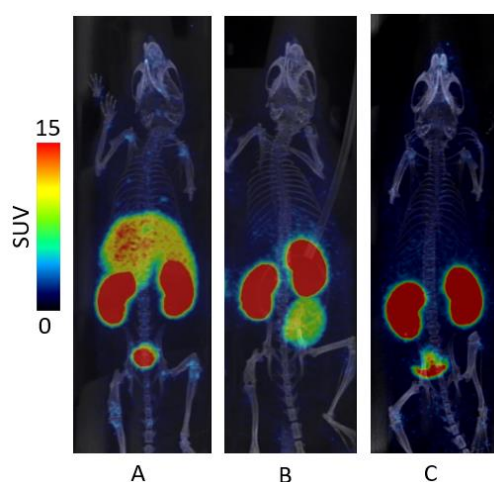


Figure 4.19: μ PET/CT study of healthy male mice. Averaged baseline image 50-60 min after injection of [¹⁸F]AIF-NOTA-DV1-K-(DV3). (1) Naïve mouse; (2) Blocked with 2.5 mg AMD3100/kg body weight; (3) Blocked with 5.0 mg AMD3100/kg body weight. Results presented as standardized uptake values (SUV).

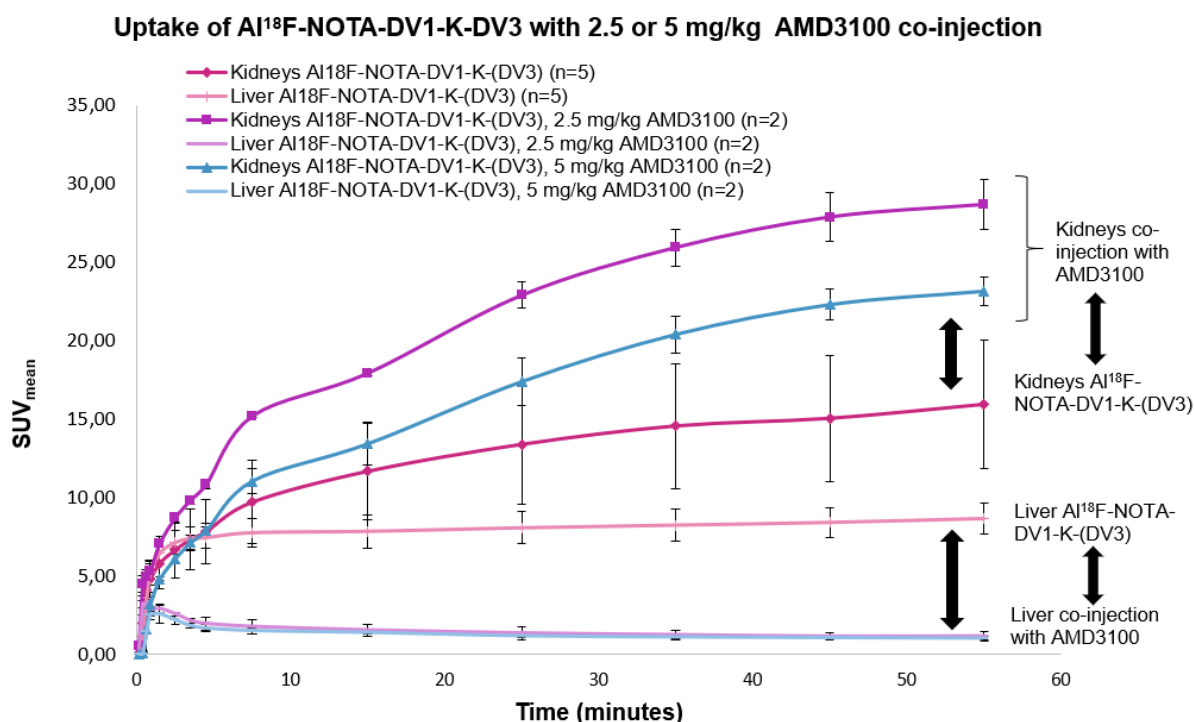


Figure 4.20: Mean SUV in different organs. The mean SUV is the average SUV within a region of interest (g/mL)(68). Five mice were injected with ^{18}F AI18F-DOTA-DV1-K-(DV3) (naïve mice), four more were injected simultaneously with ^{18}F AI18F-DOTA-DV1-K-(DV3) and the CXCR4-blocker AMD3100 (blocked mice). The average of the two concentrations of ADM3100 (2.5 mg/kg body weight and 5 mg/kg body weight) was used. SUV is plotted against the time (min).

4.7.2. Biodistribution study

The purified ^{18}F AI18F-NOTA-DV1-K-(DV3) had a yield of 1.07 GBq, and a radiochemical purity of > 95%. A biodistribution study was performed at 75 min p.i. to be able to determine the SUV in several organs more accurately than is possible in $\mu\text{PET}/\text{CT}$ scans. The data from the biodistribution study (Figure 4.21 and Table 4.3) shows high uptake in kidneys, liver, and spleen. The kidneys also had a high uptake, however adding blocking agent did not decrease the amount of activity in the kidneys. The amount of activity decreased in liver, spleen, and bone when the blocking agent AMD3100 was administered together with ^{18}F AI18F-NOTA-DV1-K-(DV3). In other organs, the amount of activity stayed relatively the same (muscle, pancreas, and lungs), while in some (blood and kidneys), the amount of activity increased (Table 4.3).

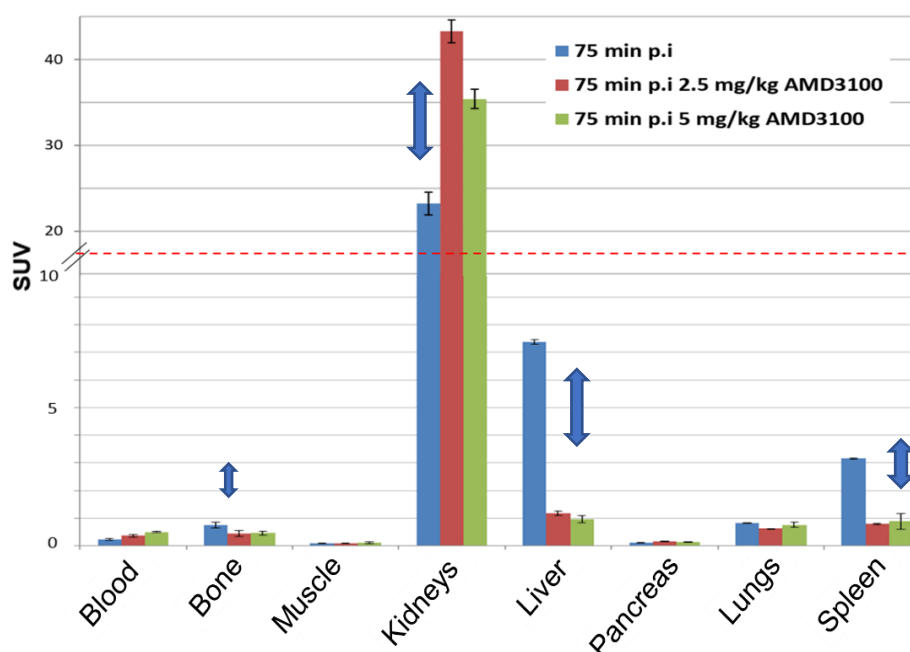


Figure 4.21: Biodistribution: Organ concentration of $[^{18}\text{F}]\text{AlF-NOTA-DV1-K-(DV3)}$ at 75 min post injection for selected organs. ($n=5$ for naïve mice, $n=2$ for each group of blocked mice (2.5 mg/kg body weight and 5 mg/kg body weight)). Values are expressed as SUV.

Table 4.3: SUV values and their standard deviation of several organs 75 min post injection of $[^{18}\text{F}]\text{AlF-NOTA-DV1-K-(DV3)}$ without blocking agent, with 2.5 mg/kg AMD3100, and with 5 mg/kg AMD3100.

$[^{18}\text{F}]\text{Al}^{18}\text{F-NOTA-DV1-K-(DV3)}$ (SUV)	75 min p.i. ($n=5$)	SD	75 min p.i. 2.5 mg/kg AMD3100 ($n=2$)	SD	75 min p.i. 5 mg/kg AMD3100 ($n=2$)	SD
Blood	0.23	0.09	0.36	0.05	0.50	0.02
Bone	0.75	0.43	0.45	0.11	0.46	0.07
Muscle	0.09	0.04	0.10	0.00	0.12	0.03
Kidneys	23.23	3.90	43.28	1.33	35.41	1.13
Liver	7.38	0.49	1.17	0.08	0.96	0.13
Pancreas	0.11	0.02	0.16	0.02	0.15	0.00
Lungs	0.83	0.22	0.63	0.00	0.76	0.09
Spleen	3.15	0.80	0.79	0.03	0.88	0.29

5. DISCUSSION

5.1. DV1-K-(DV3) PEPTIDE

Research has determined that the CXCR4 receptor is an important receptor in several pathologies, including myocardial infarcts, several infections including HIV and in oncology. Many types of tumours overexpress CXCR4, making it an important target for both imaging and treatment. The current radiopharmaceuticals cannot be used for a theranostic approach, as diagnostic and therapeutic radiopharmaceuticals have very different PK profiles. Additionally, the most clinically used CXCR4-targeting PET tracer (^{68}Ga]-Ga-Pentixafor) uses gallium-68 as radioisotope, which has several disadvantages when compared to fluorine-18. No promising fluorine-18 tracer is currently available on the market. The biggest advantage of a theranostic approach in cancer treatment is that patients can be assessed through PET imaging to quantify CXCR4 expression and predict whether (a systemic) treatment of all the cancer lesions with the accompanying therapeutic radiopharmaceutical is an option, as the tracer and the therapeutic radiopharmaceutical have a similar PK profile.

DV1-K-(DV3), a D-peptide derived from vMIP-II, is expected to have high affinity, high selectivity and high predicted *in vivo* stability due to its D-AAs composition. The final aim of this project is to translate this new class of radiopharmaceuticals into the clinic. The aim of this thesis was to start with fundamental research (development of new CXCR4 targeted radiopharmaceuticals) and to conduct part of the preclinical evaluation. The new vector molecule DV1-K-(DV3) was modified with suitable chelators in order to develop a fluorine-18 tracer (^{18}F]-AIF-NOTA/RESCA-DV1-K-(DV3)) and accompanying therapeutic radiopharmaceutical as PRRT (^{225}Ac]/ ^{177}Lu]-DOTA-DV1-K-(DV3)). Several experiments, part of the fundamental research, were carried out to examine the constructs' affinity and activity. As preclinical evaluation, radiolabelling of NOTA-DV1-K-(DV3) with ^{18}F]-AIF was carried out and the PK profile was determined *in vivo* using $\mu\text{PET}/\text{CT}$ and through *ex vivo* biodistribution in healthy mice.

In the past few decades, peptides have become a pathway of interest to the pharmaceutical industry and academia, as researchers discovered their critical role in human biology (69). Peptides are seen as more precise and specific than small molecules (70). Scaffolds based on proteins and peptides have also shown a greater capability to disrupt protein-protein interactions (71) and are more likely to be excreted through the kidneys instead of undergoing hepatic metabolism. However, there are a few downsides when working with peptides in a pharmaceutical setting. Their rapid proteolytic degradation hinders their *in vivo* efficacy through a decreased metabolic stability and lower biological availability (72).

Several methods have been developed to ensure the peptides last longer *in vivo*, such as synthetic AA substitution. This can be achieved through e.g. enantiomer AA (D-AA) substitution. This causes peptides to be more resistant to the body's proteases, due to the proteases' inability to recognize the

stereochemical reversed side-chains as substrates (71). However, one of the problems that might arise when using D-AAs instead of L-AAs is the biological activity being compromised. The D-peptide is not recognized by the proteases, but might also not be recognized by the native peptide's receptor (71).

DV1-K-(DV3) is made out of the N-terminus of vMIP-II, which was determined to be the dominant factor for CXCR4 binding when researchers performed affinity tests with certain parts of vMIP-II (58)(Figure 5.1). The N-terminus of vMIP-II (V1/DV1) binds mostly to the minor subpocket with a few polar interactions with certain AAs (58)(Figure 5.2). It was also proven that the D-peptide DV1-K-(DV3) retained a high affinity for CXCR4 and that the peptide binding site on the CXCR4-receptor has a high tolerance to changes in chirality of its ligands (56,57).

Further, the bivalent peptide DV1-K-(DV3) has an increased affinity for CXCR4 in regards to the monovalent peptides, which can be explained by the fact that the CXCR4 receptor has a binding pocket that can be divided into a minor and a major subpocket. DV1-K-(DV3) might occupy both binding subpockets simultaneously (58). DV1-K-(DV3) could be a promising new vector molecule for the development of diagnostic and therapeutic radiopharmaceuticals as it has high affinity for CXCR4, is selective for CXCR4, can be derivatised site-specifically at the C-terminus side and as it is expected to have a high metabolic stability as it is composed entirely out of D-AA's.

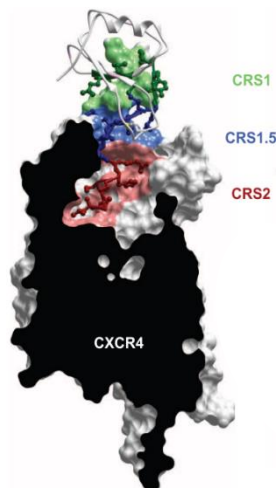


Figure 5.1: Crystal structure of the CXCR4-vMIP-II complex. CRS stands for chemokine recognition site. The green CRS1 site depicts the N-terminus of vMIP-II. Figure adapted from Qin et al. (2015)(58).

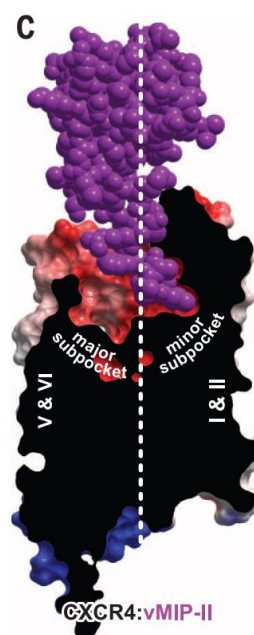


Figure 5.2: Crystal structure of the CXCR4-vMIP-II complex depicting the major and minor subpocket of CXCR4 and which parts are occupied by vMIP-II. Figure adapted from Qin et al. (2015)(58).

5.2. FUNDAMENTAL RESEARCH AND PRECLINICAL EVALUATION

The Al¹⁸F-method has the advantage that, like gallium-labelling, complexation in aqueous environment is possible. Usually, fluorine-18 has to be incorporated in molecules using harsh, water-free reaction conditions. The NOTA-chelator has a closed macrocyclic structure, while RESCA has an open acyclic structure. Al¹⁸F-complexation with NOTA gives a complex with a neutral charge but requires high temperatures (> 95°C). In contrast, Al¹⁸F-complexation with RESCA gives a complex with one negative charge and occurs at room temperature. The cold AlF-labelling was first tested using the ligand NODA-MP-NCS as such, to optimize the labelling conditions before synthesising the peptide construct AlF-NOTA-DV1-K-(DV3). The test reaction looked promising, however, the actual synthesis of AlF-NOTA-DV1-K-(DV3) was not performed yet.

The labelling with stable isotopes yielding Ga-NOTA-DV1-K-(DV3), Ga-DOTA-DV1-K-(DV3), and Lu-DOTA-DV1-K-(DV3) proceeded quantitatively with high chemical purity after C₁₈ solid-phase purification, no further (HPLC) purification was required.

The ^{nat}La³⁺-labelling of DOTA-DV1-K-(DV3) was not successful using the protocol described in 3.4.5. A possible explanation for these poor results could be that the pH that was used was too high, causing La(OH)₃ to be formed. The lanthanum that is incorporated in La(OH)₃ is unable to react with the DOTA-chelator. A protocol that performs the reaction at a lower pH would be preferable for further tests.

The affinity tests showed that the highest tested concentration of each of the constructs was not capable of inhibiting the response more than 50%. Further tests could be performed to determine which concentration would inhibit the binding by 100%. AMD3100 was used as the blocking agent, as it is the 'golden standard' when it comes to CXCR4 inhibitors, while AMD11070 is a newer and more potent inhibitor. The tests with La-DOTA, Ga- and AlF-NOTA and AlF-RESCA complexes still need to be performed. It was demonstrated by the Rega Institute that the peptides can be 'sticky' and stick to the pipette tips, which therefore need to be changed for each of the dilutions to ensure a correct concentration. The affinity curves of the cold constructs had a shape that slightly deviates from the curves obtained with the reference peptide (DV1-K-(DV3)). This may be due to the fact that the negative charges of DOTA, which had three free deprotonated carboxyl-groups, and of NOTA, which had two free deprotonated carboxyl-groups, had a negative impact on the constructs' affinity for the CXCR4 receptor. The Ga³⁺-, and Lu³⁺-DOTA complexes were neutral and had a curve that did not deviate from the curve of the reference peptide. The changes in charge of the complex could affect the affinity, as the CXCR4 receptor is negatively charged (58)(a negative charge of -9 (57)). However, previous studies (see Zhou *et al.* (2002)(57)) have shown that a wide variety of ligands can bind CXCR4, each with widely different charges ranging from +2.5 to +9. These ligands are presumed to bind through electrostatic interactions, but the receptor is not sensitive to changes in overall positive charge of the

ligand, indicating at least partial non-specific binding of CXCR4 by its ligands. (DV1 has an overall charge of +3.5)(57). The La³⁺-DOTA, Ga³⁺- and AIF-NOTA and AIF-RESCA would also be neutral, while the AIF-RESCA complex would have a negative overall charge. One could remark that the affinity test might better be named an inhibitory activity test, due to the fact that the test measures the % of inhibition of CXCL12 binding to the CXCR4 receptor.

The calcium-binding assay shows an inhibition of the calcium release when a higher concentration of a construct was added. All constructs are able to inhibit the calcium release, though they do not have the same activity. AMD11070 is the most potent antagonist, followed by AMD3100, DV1-K-(DV3), NOTA-DV1-K-(DV3), Ga-DOTA-DV1-K-(DV3), DOTA-DV1-K-(DV3), and lastly Lu-DOTA-DV1-K-(DV3). The tests with the La³⁺-DOTA, Ga³⁺- and AIF-NOTA and AIF-RESCA complexes were also not performed due to unforeseen circumstances.

While developing the QC system, more than one peak was observed after injecting the reference (DV1-K-(DV3) 1 mg/mL in H₂O/ACN 50/50 v/v%). This might be due to degradation, as the aliquots were kept in the freezer for a few months and the same aliquot was continuously thawed and refrozen to inject the next run. A fresh aliquot seemed to reduce one of the peaks, indicating it might be a degradation product that was seen on the run. Though the retention time of DV1-K-(DV3) was favourable, the peak shape can still be improved, as it was quite broad. Using a C₃ column might solve this problem, as the lipophilic peptide will have less interaction with the stationary phase. Another possible solution is to shift towards a HPLC system using a gradient of water and ACN with 0.1% TFA (pH 2-3), this acidic system is used often for the analysis and purification of peptides. However, Ory *et al.* (2015) previously demonstrated that when using a mobile phase with a low pH on a silica-based C₁₈-column, retention of free ¹⁸F⁻ in the form of H¹⁸F can result in an overestimation of the radiochemical purity during QC. A solution to overcome this problem is to shift towards a polymer-based column instead of a silica-based column.

The [¹⁸F]AIF-NOTA-DV1-K-(DV3) μPET/CT scans of the naïve mice showed high activity in the kidneys, bladder, and liver. It demonstrated rapid renal clearance, which is positive due to the fact that rapid clearance from the blood and renal clearance causes a higher contrast to the rest of the body. Its accumulation in the bladder and kidneys does mean that it would not be a suitable tracer for the detection and follow up of bladder or kidney cancer. The lack of uptake in most other tissues (e.g. muscle) may indicate that the tracer would deliver high-contrast images and could be used for a variety of cancers in multiple organs. When the blocking agent AMD3100 was used, the uptake in the liver decreased and the uptake in the kidneys increased. This is indicative of a specific binding of [¹⁸F]AIF-NOTA-DV1-K-(DV3) to the CXCR4 receptor, which is expressed most notably in the liver in healthy mice. When the tracer is blocked from binding to the CXCR4 receptor, the tracer is excreted more rapidly through the kidneys, causing a higher kidney SUV.

In the biodistribution data, the tail is not taken into account in the calculation of the %ID, because a more lipophilic substance can stick to the tissue and cause the data to be skewed and generate wrong PK values. The SUV normalises the concentration of radioactivity to the injected radioactive dose and the body weight of the animal or person. If the SUV has a value of one, the concentration of the radiotracer would be equal to the concentration that would theoretically be expected if the tracers distributes homogenously throughout the body (73). The data from the biodistribution study in healthy mice shows that the organs with the highest CXCR4-expression are the spleen and liver. The kidneys also had a high uptake, however adding blocking agent did not decrease the amount of activity in the kidneys, but instead increased the activity in the kidneys, indicating that the uptake is caused by excretion of the radiotracer via the kidneys to the bladder and not due to CXCR4-related binding.

The bone uptake is an important marker in fluorine-18 tracers to assess the biological stability of the construct. However, CXCR4 is also expressed in the bone marrow. The data shows only moderate uptake of in the bones, indicating a good stability of the tracer. The data from the biodistribution study wherein a CXCR4 receptor blocking agent AMD3100 was used, strongly suggest that the tracer is specific for the CXCR4 receptor. This is due to the lower activity concentration measured in liver, spleen and, although less pronounced, bone. It is known that the CXCR4 receptor is expressed in these organs in healthy mice. The difference between the two doses of blocking agent (2.5 mg AMD3100/kg body weight and 5 mg AMD3100/kg body weight) is not very pronounced.

To conclude, [¹⁸F]AIF-NOTA-DV1-K-(DV3) shows *in vivo* CXCR4 specificity and promising PK properties with fast plasma clearance and urinary excretion, resulting in a high tissue-to-background ratio. This high tissue-to-background ratio will result in high signal-to-noise PET images and a potentially higher selectivity of irradiation of tumours when using the therapeutic radiopharmaceuticals. Finally, DV1-K-(DV3) has shown high affinity for both mouse and human CXCR4, which makes it promising for further translational research.

5.3. FUTURE STEPS

Due to the unforeseen COVID-19 lockdown, several experiments were not performed yet. The lab of Radiopharmaceutical research at KU Leuven will perform these experiments in the future to further evaluate the potential of DV1-K-(DV3) as a suitable vector for theranostic radiopharmaceuticals.

Further affinity tests and calcium-binding assays will be performed after synthesis of the remaining constructs: Ga-NOTA-DV1-K-(DV3), RESCA-DV1-K-(DV3), AIF-RESCA-DV1-K-(DV3), FITC-DV1-K-(DV3), and La-DOTA-DV1-K-(DV3). The Rega Institute will also perform CXCR7-binding tests to determine whether the modifications made to the constructs cause them to bind to CXCR7, while it was already established that DV1-K-(DV3) does not bind to CXCR7. Cell binding and internalisation

studies will also be performed with [¹⁸F]AIF-NOTA-DV1-K-(DV3) on U87.CXCR4 cells, to investigate the binding affinity constant, thereby indicating whether the constructs are internalised after binding to CXCR4. RESCA will be tested as a chelator, as it requires less harsh reaction conditions (lower temperature) for the radiolabelling of the construct which is convenient for clinical translation. However, preliminary data indicates the change in overall charge (-1 vs neutral) in comparison to NOTA might not yield a construct with high affinity. The change in charge might cause the affinity to drop well below the affinity of AIF-NOTA-DV1-K-(DV3) and additionally, the RESCA-chelator would make the construct more lipophilic. This could result in less favourable PK properties such as a combination of renal and hepatic clearance. First proof-of-concept radiolabelling of DOTA-DV1-K-(DV3) with ¹⁷⁷Lu, ²²⁵Ac and ⁶⁸Ga will be performed, as well as proof-of-concept radiolabelling of NOTA-DV1-K-(DV3) with ⁶⁸Ga.

Radiometabolite studies (in urine and in plasma) will be performed to confirm the expected high metabolic stability. The constructs should be stable in plasma without formation of radiometabolites to ensure they reach their target.

Two tumour models will also be developed in cooperation with the Molecular Small Animal Imaging Center (MoSAIC) of KU Leuven. Both a CXCR4-positive xenograft and a CXCR4-positive multiple myeloma mouse model will be developed to test the *in vivo* properties of both the diagnostic and therapeutic radiopharmaceuticals in relevant animal models. First, [¹⁸F]AIF-NOTA-DV1-K-(DV3) will be compared to [⁶⁸Ga]Ga-Pentixafor as a baseline. These tests will be performed both with and without blocking using 5 mg AMD3100/kg body weight. Next, therapeutic efficacy studies will also be performed in the same animal models in a theranostic approach (34).

Finally, for translation to a clinical setting, toxicity studies will be required and the QC HPLC system will be optimized, ensuring that further translation to a clinical setting will be possible.

6. CONCLUSION

The preliminary results of the *in vivo* and *in vitro* studies show promising results for the DV1-K-(DV3) vector as a CXCR4-targeting radiopharmaceutical. The bivalent peptide, consisting of only D-amino acids, has a high affinity for CXCR4 and is expected to have a high metabolic stability, making it a suitable vector molecule for radiopharmaceuticals. *In vivo* studies on healthy mice using [¹⁸F]AlF-NOTA-DV1-K-(DV3) have indicated good pharmacokinetic properties of the fluorine-18 tracer with rapid renal clearance and high and specific binding towards CXCR4 expressing tissues. As there is no good fluorine-18 tracer targeting CXCR4 on the market yet, these positive properties indicate its potential to fill this unmet medical need. Further testing is necessary to determine whether the vector could also be used in a theranostic approach.

7. LITERATURE CITED

1. World Nuclear Association. What Is Background Radiation? World Nuclear Association;
2. MedicalNewsToday. What is nuclear medicine? [Internet]. [cited 2020 Mar 5]. Available from: <https://www.medicalnewstoday.com/articles/248735>
3. Vermeulen K, Vandamme M, Bormans G, Cleeren F. Design and Challenges of Radiopharmaceuticals. *Semin Nucl Med.* 2019;49(5):339–56.
4. Kostelnik TI, Orvig C. Radioactive Main Group and Rare Earth Metals for Imaging and Therapy. *Chem Rev.* 2019;119:902–56.
5. Colombetti LG. Principles of radiopharmacology Volume I. 1st ed. Colombetti LG, editor. Boca Raton: CRC press; 1979.
6. Jewett DM, Kilbourn MR. In vivo evaluation of new carfentanil-based radioligands for the mu opiate receptor. *Nucl Med Biol.* 2004;31:321–5.
7. Science & Technology - Facilities Council. 2. Isotopes and decay - Decay equations [Internet]. [cited 2019 Sep 24]. p. 9. Available from: <http://resources.schoolscience.co.uk/stfc/16plus/partich2pg4.html>
8. Tro N. 20.4: The Valley of Stability- Predicting the Type of Radioactivity [Internet]. 2019 [cited 2020 Jan 15]. Available from: [https://chem.libretexts.org/Bookshelves/General_Chemistry/Map%3A_A_Molecular_Approach_\(Tro\)/20%3A_Radioactivity_and_Nuclear_Chemistry/20.04%3A_The_Valley_of_Stability-_Predicting_the_Type_of_Radioactivity](https://chem.libretexts.org/Bookshelves/General_Chemistry/Map%3A_A_Molecular_Approach_(Tro)/20%3A_Radioactivity_and_Nuclear_Chemistry/20.04%3A_The_Valley_of_Stability-_Predicting_the_Type_of_Radioactivity)
9. Zalutsky MR, Pruszynski M. Astatine-211: Production and Availability. *Curr Radiopharm.* 2012;4(3):177–85.
10. Navarro-Teulon I, Lozza C, Pèlegri A, Vivès E, Pouget JP. General overview of radioimmunotherapy of solid tumors. *Immunotherapy.* 2013;5(5):467–87.
11. Conti M, Eriksson L. Physics of pure and non-pure positron emitters for PET: A review and a discussion. *EJNMMI Phys.* 2016;3(8).
12. Scheinberg DA, McDevit MR. Actinium-225 in targeted alpha-particle therapeutic applications. *Curr Radiopharm.* 2011;4(4):306–20.
13. Kassis AI. Molecular and cellular radiobiological effects of Auger emitting radionuclides. *Radiat Prot Dosimetry.* 2011;143(2–4):241–7.
14. Strategic Alliance Holdings Global LLC (“SAH Global”). PET & Molecular Imaging [Internet]. [cited 2019 Sep 26]. Available from: <https://www.sahglobal.com/pet-molecular-imaging/>
15. Suridjan I, Comley RA, Rabiner EA. The application of positron emission tomography (PET) imaging in CNS drug development. *Brain Imaging Behav.* 2019;13(2):354–65.
16. Sanchez-Crespo A. Comparison of Gallium-68 and Fluorine-18 imaging characteristics in positron emission tomography. *Appl Radiat Isot.* 2013;76:55–62.
17. Courses.Washington.edu. How it works: Positron Emission.
18. Connor N. What is Interaction of Beta Radiation with Matter - Definition [Internet]. 2019 [cited 2020 Jan 31]. Available from: <https://www.periodic-table.org/what-is-interaction-of-beta-radiation-with-matter-definition/>
19. Fornell D. SPECT Scanner vs. PET, Which is Best? [Internet]. *Diagnostic and Interventional Cardiology.*

- 2008 [cited 2020 Apr 27]. Available from: <https://www.dicardiology.com/article/spect-scanner-vs-pet-which-best>
20. Barbalace K. Periodic Table of Elements - Fluorine - F [Internet]. 2019 [cited 2019 Sep 23]. Available from: <https://environmentalchemistry.com/yogi/periodic/F.html>
 21. WebElements. WebElements Periodic Table » Fluorine » the essentials [Internet]. [cited 2019 Sep 23]. Available from: <https://www.webelements.com/fluorine/>
 22. Christé V, Bé MM, Kuzmenko NK. Fluorine-18 [Internet]. Laboratoire National Henri Becquerel/ CEA. Inhb.fr; [cited 2019 Oct 19]. Available from: <http://www.inhb.fr/nuclear-data/nuclear-data-table/>
 23. Cleeren F, Lecina J, Ahamed M, Raes G, Devoogdt N, Caveliers V, McQuade P, Rubins DJ, Li W, Verbruggen A, Xavier C, Bormans G. Al18F-labeling of heat-sensitive biomolecules for positron emission tomography imaging. *Theranostics*. 2017;7(11):2924–39.
 24. Pouget JP, Navarro-Teulon I, Bardiès M, Chouin N, Cartron G, Pèlegri A, Azria D. Clinical radioimmunotherapy - the role of radiobiology. *Nat Rev Clin Oncol*. 2011;8(12):720–34.
 25. Kassis AI. Molecular and cellular radiobiological effects of Auger emitting radionuclides. *Radiat Prot Dosimetry*. 2011;143:241–7.
 26. Baum RP. *Therapeutic Nuclear Medicine* [Internet]. 1st ed. Baum RP, editor. Heidelberg: Springer-Verlag Berlin Heidelberg; 2014. (Medical Radiology). Available from: <http://link.springer.com/10.1007/978-3-540-36719-2>
 27. Barbalace K. Periodic Table of Elements - Lutetium - Lu [Internet]. 2019 [cited 2019 Sep 23]. Available from: <https://environmentalchemistry.com/yogi/periodic/Lu.html>
 28. WebElements. WebElements Periodic Table » Lutetium » the essentials [Internet]. [cited 2019 Sep 23]. Available from: <https://www.webelements.com/lutetium/>
 29. Barbalace K. Periodic Table of Elements - Actinium - Ac [Internet]. 2019 [cited 2019 Sep 23]. Available from: <https://environmentalchemistry.com/yogi/periodic/Ac.html>
 30. WebElements. WebElements Periodic Table » Actinium » the essentials [Internet]. [cited 2019 Sep 23]. Available from: <https://www.webelements.com/actinium/>
 31. Deal KA, Davis IA, Mirzadeh S, Kennel SJ, Brechbiel MW. Improved in vivo stability of actinium-225 macrocyclic complexes. *J Med Chem*. 1999;42:2988–92.
 32. Jaggi JS, Kappel BJ, McDevitt MR, Sgouros G, Flombaum CD, Cabassa C, Scheinberg DA. Efforts to control the errant products of a targeted in vivo generator. *Cancer Res*. 2005;65(11):4888–95.
 33. Barbalace K. Periodic Table of Elements - Lanthanum - La [Internet]. 2019 [cited 2019 Sep 23]. Available from: <https://environmentalchemistry.com/yogi/periodic/La.html>
 34. Wilson DJ. What is Theranostics? [Internet]. News Medical Life Sciences. 2018 [cited 2020 Apr 27]. Available from: <https://www.news-medical.net/health/What-is-Theranostics.aspx>
 35. Pene F, Courtine E, Cariou A, Mira J-P. Toward theragnostics. *Crit Care Med*. 2009;37(SUPPL. 1):S50–8.
 36. Sathekge M. Targeted radionuclide therapy. *Contin Med Educ J*. 2013;31(8):289–94.
 37. Gudkov S V., Shilyagina NY, Vodenev VA, Zvyagin A V. Targeted radionuclide therapy of human tumors. *Int J Mol Sci*. 2015;17(1).
 38. Hughes CE, Nibbs RJB. A guide to chemokines and their receptors. *FEBS J*. 2018;285(16):2944–71.

39. Kircher M, Herhaus P, Schottelius M, Buck AK, Werner RA, Wester H-JJ, Keller U, Lapa C. CXCR4-directed theranostics in oncology and inflammation. *Ann Nucl Med*. 2018;32(8):503–11.
40. Bernhagen J, Krohn R, Lue H, Gregory JL, Zerneck A, Koenen RR, Dewor M, Georgiev I, Schober A, Leng L, Kooistra T, Fingerle-Rowson G, Ghezzi P, Kleemann R, McColl SR, Bucala R, Hickey MJ, Weber C. MIF is a noncognate ligand of CXC chemokine receptors in inflammatory and atherogenic cell recruitment. *Nat Med*. 2007;13(5):587–96.
41. Pawig L, Klasen C, Weber C, Bernhagen J, Noels H. Diversity and Inter-Connections in the CXCR4 Chemokine Receptor/Ligand Family: Molecular Perspectives. *Front Immunol*. 2015;6(429).
42. The Liotta Research Group, Liotta D. CXCR4 AND CCR5 [Internet]. [cited 2020 Jan 17]. Available from: <https://scholarblogs.emory.edu/liotta/projects/cxcr4/>
43. Feng Y, Broder CC, Kennedy PE, Berger EA. HIV-1 Entry Cofactor: Functional cDNA Cloning of a Seven-Transmembrane, G Protein-Coupled Receptor. *Science* (80-). 1996;272(5263):872–7.
44. Thackeray JT, Derlin T, Haghikia A, Napp LC, Wang Y, Ross TL, Schäfer A, Tillmanns J, Wester HJ, Wollert KC, Bauersachs J, Bengel FM. Molecular Imaging of the Chemokine Receptor CXCR4 after Acute Myocardial Infarction. *JACC Cardiovasc Imaging*. 2015;8(12):1417–26.
45. Sun X, Cheng G, Hao M, Zheng J, Zhou X, Zhang J, Taichman RS, Pienta KJ, Wang J. CXCL12 / CXCR4 / CXCR7 chemokine axis and cancer progression. *Cancer Metastasis Rev*. 2010;29(4):709–22.
46. Tsutsumi H, Tanaka T, Ohashi N, Masuno H, Tamamura H, Hiramatsu K, Araki T, Ueda S, Oishi S, Fujii N. Therapeutic Potential of the Chemokine Receptor CXCR4 Antagonists as Multifunctional Agents. *Wiley Intersci*. 2007;88(2):279–89.
47. Boulais PE, Dulude D, Cabana J, Heveker N, Escher E, Lavigne P, Leduc R. Photolabeling identifies transmembrane domain 4 of CXCR4 as a T140 binding site. *Biochem Pharmacol*. 2009;78:1382–90.
48. Wester HJ, Keller U, Schottelius M, Beer A, Philipp-Abbrederis K, Hoffmann F, Šimeček J, Gerngross C, Lassmann M, Herrmann K, Pellegata N, Rudelius M, Kessler H, Schwaiger M. Disclosing the CXCR4 expression in lymphoproliferative diseases by targeted molecular imaging. *Theranostics*. 2015;5(6):618–30.
49. Poschenrieder A, Schottelius M, Schwaiger M, Kessler H, Wester HJ. The influence of different metal-chelate conjugates of pentixafor on the CXCR4 affinity. *EJNMMI Res*. 2016;6.
50. George GPC, Pisaneschi F, Nguyen QD, Aboagye EO. Positron emission tomographic imaging of CXCR4 in cancer: challenges and promises. *Mol Imaging*. 2014;13.
51. Schottelius M, Osl T, Poschenrieder A, Hoffmann F, Beykan S, Hänscheid H, Schirbel A, Buck AK, Kropf S, Schwaiger M, Keller U, Lassmann M, Wester HJ. [¹⁷⁷Lu]pentixather: Comprehensive preclinical characterization of a first CXCR4-directed endoradiotherapeutic agent. *Theranostics*. 2017;7(9):2350–62.
52. Poschenrieder A, Osl T, Schottelius M, Hoffmann F, Wirtz M, Schwaiger M, Wester H. First ¹⁸F-Labeled Pentixafor-Based Imaging Agent for PET Imaging of CXCR4 Expression In Vivo. *Tomography*. 2016;2(2):85–93.
53. Habringer S, Lapa C, Herhaus P, Schottelius M, Istvanffy R, Steiger K, Slotta-Huspenina J, Schirbel A, Hänscheid H, Kircher S, Buck AK, Götze K, Vick B, Jeremias I, Schwaiger M, Peschel C, Oostendorp R, Wester H-J, Grigoleit G-U et al. Dual Targeting of Acute Leukemia and Supporting Niche by CXCR4-Directed Theranostics. *Theranostics*. 2018;8(2):369–83.

54. Maurer S, Herhaus P, Lippenmeyer R, Hänscheid H, Kircher M, Schirbel A, Maurer CH, Buck AK, Wester H-J, Einsele H, Grigoleit G-U, Keller U, Lapa C. Side effects of CXC-chemokine receptor 4-directed endoradiotherapy with pentixather before hematopoietic stem cell transplantation. *J Nucl Med.* 2019;60:1399–405.
55. Mao Y, Meng Q, Song P, Zhu S, Xu Y, Snyder EY, An J, Huang Z. Novel Bivalent and D-Peptide Ligands of CXCR4 Mobilize Hematopoietic Progenitor Cells to the Blood in C3H/HeJ Mice. *Cell Transplant.* 2018;27(8):1249–55.
56. Xu Y, Duggineni S, Espitia S, Richman DD, An J, Huang Z. A synthetic bivalent ligand of CXCR4 inhibits HIV infection. *Biochem Biophys Res Commun.* 2013;435:646–50.
57. Zhou N, Luo Z, Luo J, Fan X, Cayabyab M, Hiraoka M, Liu D, Han X, Pesavento J, Dong C-Z, Wang Y, An J, Kaji H, Sodroski JG, Huang Z. Exploring the stereochemistry of CXCR4-peptide recognition and inhibiting HIV-1 entry with D-peptides derived from chemokines. *J Biol Chem.* 2002;277(20):17476–85.
58. Qin L, Kufareva I, Holden LG, Wang C, Zheng Y, Zhao C, Fenalti G, Wu H, Han GW, Cherezov V, Abagyan R, Stevens RC, Handel TM. Crystal structure of the chemokine receptor CXCR4 in complex with a viral chemokine. *Science (80-).* 2015;347(6226):1117–22.
59. Zhou N, Luo Z, Luo J, Hall JW, Huang Z. A Novel Peptide Antagonist of CXCR4 Derived from the N-Terminus of Viral Chemokine vMIP-II. *Biochemistry.* 2000;39:3782–7.
60. American Cancer Society. Getting Oral or Systemic Radiation Therapy [Internet]. 2019 [cited 2020 Feb 28]. Available from: <https://www.cancer.org/treatment/treatments-and-side-effects/treatment-types/radiation/systemic-radiation-therapy.html>
61. MinFound Medical Systems. PET scanner / CT scanner / for full-body tomography / 16-slice [Internet]. [cited 2020 May 7]. Available from: <https://www.medicalexpo.com/prod/minfound-medical-systems/product-122176-857419.html>
62. Cleeren F, Lecina J, Bridoux J, Devoogdt N, Tshibangu T, Xavier C, Bormans G. Direct fluorine-18 labeling of heat-sensitive biomolecules for positron emission tomography imaging using the A118F-RESCA method. *Nat Protoc.* 2018;13(10):2330–47.
63. Suzuki K, Ui T, Nagano A, Hino A, Arano Y. C-terminal–modified LY2510924: a versatile scaffold for targeting C-X-C chemokine receptor type 4. *Nat Sci reports.* 2019;9(1):1–8.
64. Ucar B. Synthesis and characterization of natural lanthanum labelled DOTA-Peptides for simulating radioactive Ac-225 labeling. *Appl Radiat Isot.* 2019;153.
65. Schoofs G, Van Hout A, D’huys T, Schols D, Van Loy T. A flow cytometry-based assay to identify compounds that disrupt binding of fluorescently-labeled CXC chemokine ligand 12 to CXC chemokine receptor 4. *J Vis Exp.* 2018;(e57271).
66. Claes S, D’huys T, Van Hout A, Schols D, Van Loy T. A kinetic fluorescence-based Ca²⁺ mobilization assay to identify G protein-coupled receptor agonists, antagonists, and allosteric modulators. *J Vis Exp.* 2018;132.
67. Bergström M, Grahnén A, Långström B. Positron emission tomography microdosing: a new concept with application in tracer and early clinical drug development. p. 357–366.
68. Kinahan PE, Fletcher JW. PET/CT Standardized Uptake Values (SUVs) in Clinical Practice and Assessing Response to Therapy. *Natl Inst Heal.* 2010;31(6):496–505.

69. Fosgerau K, Hoffmann T. Peptide therapeutics: current status and future directions. *Drug Discov Today*. 2015;20(1):122–8.
70. Meister D, Taimoory SM, Trant JF. Unnatural amino acids improve affinity and modulate immunogenicity: Developing peptides to treat MHC type II autoimmune disorders. *Pept Sci*. 2019;111.
71. Werner HM, Cabaltega CC, Horne WS. Peptide Backbone Composition and Protease Susceptibility: Impact of Modification Type, Position, and Tandem Substitution. *ChemBioChem*. 2016;17(8):712–8.
72. Lee AC-L, Harris JL, Khanna KK, Hong J-H. A Comprehensive Review on Current Advances in Peptide Drug Development and Design. *Int J Mol Sci*. 2019;20(2383).
73. Pike VW. PET Radiotracers: crossing the blood-brain barrier and surviving metabolism. *Trends Pharmacol Sci*. 2009;30(8):431–40.
74. thyroidcancersurvivor. What is Cancer? [Internet]. 2010 [cited 2020 May 18]. Available from: <https://thyroidcancersurvivor.wordpress.com/2010/10/13/what-is-cancer/>

